

DIJET RAPIDITY GAPS IN PHOTOPRODUCTION FROM PERTURBATIVE QCD

GIANLUCA ODERDA

*Institute for Theoretical Physics
State University of New York at Stony Brook
Stony Brook, NY 11794-3840, USA*

Abstract

By defining dijet rapidity gap events according to interjet energy flow, we treat the photoproduction cross section of two high transverse momentum jets with a large intermediate rapidity region as a factorizable quantity in perturbative QCD. We show that logarithms of soft gluon energy in the interjet region can be resummed to all orders in perturbation theory. The resummed cross section depends on the eigenvalues of a set of soft anomalous dimension matrices, specific to each underlying partonic process, and on the decomposition of the scattering according to the possible patterns of hard color flow. We present a detailed discussion of both. Finally, we evaluate numerically the gap cross section and gap fraction and compare the results with ZEUS data. In the limit of low gap energy, good agreement with experiment is obtained.

PACS Nos.: 12.38.Aw, 12.38.Cy, 13.85.-t, 13.87.-a

1 Introduction

In a recent paper [1] we have presented an explanation, from perturbative QCD, of the dijet rapidity gap events experimentally observed in $p\bar{p}$ scattering at the Fermilab Tevatron [2]. These events consist of a pair of jets produced at very large momentum transfer, and separated by a wide empty region, where barely any particle multiplicity is measured. They were originally predicted from the exchange of at least two gluons in a color singlet configuration, which avoids color recombination between the jets and associated interjet hadronization [3]. A quantitative formalism to describe gap events, however, has been lacking in the literature.

In Ref. [1] we have discussed the dependence of the dijet cross section on the energy flow into the central region, clearly related to the observed particle multiplicity. We have shown how to factorize the partonic cross section into a hard scattering function, accounting for the dynamics of the highly virtual quanta exchanged in the scattering, and a soft function, describing the soft radiation emitted into the interjet region. Both functions are defined as matrices in the space of the possible color flows at the hard scattering, formalizing the idea, already expressed by other authors, that the color structure of the short-distance partonic scattering is not uniquely defined [4, 5]. The soft function contains, at each order in perturbation theory, logarithms of the interjet radiation energy, which can be resummed, to give the dependence of the dijet cross section on the interjet energy flow. The resummation is driven by the eigenvalues and eigenvectors of a soft anomalous dimension matrix, defined in the space of color flows. In Ref. [1], we have performed the analysis of this matrix for $q\bar{q} \rightarrow q\bar{q}$ scattering, which is the relevant partonic process in a valence quark approximation for $p\bar{p}$ collisions. The result indicates that, in the limit of a very large interjet region (corresponding to a very large parton center of mass energy, compared to the momentum transfer), the color singlet component dominates, thus merging our picture, in this asymptotic configuration, with approaches to the problem based on the Regge limit of QCD [6] and on the idea of color singlet dominance [3, 7]. We have already pointed out that a full treatment of the Tevatron dijet gap cross section requires us to include the contribution of processes involving gluons, which we postpone, for that specific problem, to forthcoming work [8].

In this paper, we will apply our method to analyze the photoproduction of two high transverse momentum jets with a large intermediate rapidity gap. Events of this kind have been reported in e^+p collisions at HERA [9]. Here, the quantity of interest is the gap fraction, the ratio of the number of dijet events with a large interjet gap, to the total number of dijet events. The ZEUS experiment shows that, binning the gap events according to the width of the interjet empty region, the gap fraction, after an initial decay, reaches an asymptotic plateau. It has been shown in Refs. [3, 6] that the fraction of gap events from the exchange of a color octet, reggeized gluon falls off exponentially with increasing gap width. The left-over asymptotic excess has been interpreted as the fraction of the color singlet exchange of a hard BFKL pomeron [6]. We emphasize here that the BFKL approach is complementary to ours, because it deals with the resummation of gluonic radiation, which, in our language, would be described as hard (see Sec. 6 below).

Applying the methods of Ref. [1] to this problem is especially interesting, because, while the data for the Tevatron gaps show the dependence of the cross section on the interjet energy at fixed gap width, here we will explore the opposite dependence, variable gap width at fixed energy. We will show that the factorization and resummation of the soft gluonic energy emitted into the gap leads precisely to the behavior of the gap fraction observed by the experiment. In addition, photoproduction is an ideal process in which to analyze the contribution of gluons to gap cross sections. Theoretical studies of jet photoproduction have been pursued since the early 80's [10, 11, 12, 13, 14, 15] and are a very active area of research. The dominant partonic mechanisms in photoproduction are the direct and resolved scatterings: in the former case the photon from the incoming lepton interacts directly with the quark or gluon from the proton, and in the latter it fluctuates first into a hadronic state of low virtuality, acting as a source of partons, which then scatter off partons from the proton. The precise experimental determination of the partonic content of the photon is still an open problem, partly because it requires isolating the resolved component of the scattering [10, 16]. However, existing data indicate that, especially at low values of partonic x , the dominant component of the photon is gluonic [12]. Correspondingly, we will see that for the resolved contribution, the scattering of a gluon from the photon with a quark from the proton is dominant in the kinematical region of interest. Also the contribution from the resolved reaction $g + g \rightarrow g + g$ has to be taken into account, although it turns out to be much less important in this case, because of the high transverse energy cuts experimentally imposed on the jets.

One last important remark has to be made, about the issue of survival [3, 17]. In dijet gap events, the survival probability is limited by the probability of no radiation inside the gap from the interaction of spectator partons. Such probability is estimated to be of the order of 10% in $p\bar{p}$ scattering, if we require a truly empty interjet region [3, 17]. Presumably, for ep reactions the number of spectator quarks and gluons is reduced with respect to $p\bar{p}$ scattering, because of the partly leptonic nature of the initial state. Therefore our resummed formula, which accounts for the amount of perturbative survival from soft gluon dynamics, should be less sensitive to these effects.

Throughout the paper, we will work in close correspondence with the ZEUS experimental configuration described in Ref. [9]. In Sec. 2, we will discuss the kinematics of the problem, define the dijet gap cross section, and review its factorization properties. In Sec. 3, we will introduce the gap fraction, as the ratio of the dijet gap cross section to the overall dijet cross section. We will also identify the partonic reactions giving the largest contributions to both the gap and the overall cross section. For each of these reactions, in Sec. 4, we will present the explicit decomposition into hard and soft parts. In Sec. 5, we will present the process-dependent soft anomalous dimension matrices, their eigenvalues and eigenvectors, which govern the soft dynamics of the scattering. Finally, in Sec. 6, we will give numerical results for the overall dijet cross section, the dijet gap cross section and the gap fraction. We will draw a comparison with the experimental results of Ref. [9], and present our conclusions.

2 Dijet Gap Cross Sections in Photoproduction

2.1 Definitions

In this section we will introduce dijet gap cross sections in photoproduction. We first recall the definition of particle pseudorapidity,

$$\eta = \ln \left(\cot \left(\frac{\theta}{2} \right) \right), \quad (1)$$

where θ is the angle of a particle momentum with respect to a fixed direction, typically the beam direction. We will consider positron-proton scattering

$$e^+(p_A) + p(p_B) \longrightarrow e^+(p'_A) + J_1(p_1) + J_2(p_2) + X_{\text{gap}}, \quad (2)$$

for the production of two jets at fixed pseudorapidity difference, $\Delta\eta = \eta_1 - \eta_2$. We sum inclusively over final states, while measuring the (soft) energy flow into the intermediate region between the jets. The boost-invariant pseudorapidity difference $\Delta\eta$ fixes the partonic scattering angle $\hat{\theta}$ through the formula

$$\frac{\Delta\eta}{2} = \ln \left(\cot \left(\frac{\hat{\theta}}{2} \right) \right). \quad (3)$$

Following Ref. [9], the jets are defined by cones of radius $R = 1.0$ in the η - ϕ plane mapping the ZEUS calorimeter detector. This constrains the interjet region to have (pseudo)rapidity width

$$\Delta y = \Delta\eta - 2R. \quad (4)$$

The low-virtuality photons exchanged at the electromagnetic vertex of the interaction can be thought of as real particles of energy $E_\gamma = yE_e$, whose spectrum is given by the Weiszäcker-Williams formula [18, 19]

$$F_{\gamma/e}(y) = \frac{\alpha_{\text{em}}}{2\pi} \left\{ \frac{1 + (1-y)^2}{y} \ln \left(\frac{Q_{\text{max}}^2(1-y)}{m_e^2 y^2} \right) + 2m_e^2 y \left[\frac{1}{Q_{\text{max}}^2} - \frac{(1-y)}{m_e^2 y^2} \right] \right\}. \quad (5)$$

Here α_{em} is the electromagnetic coupling, m_e is the electron mass, and Q_{max}^2 is the maximum photon virtuality, determined from the (anti) tagging conditions of the experiment. From Ref. [9] we take the value $Q_{\text{max}}^2 = 4\text{GeV}^2$. The generic differential cross section for electron-proton scattering can then be viewed as a convolution of the photon distribution in the electron and the photon-proton cross section:

$$d\sigma_{ep}(S) = \int_{y_{\text{min}}}^{y_{\text{max}}} dy F_{\gamma/e}(y) d\sigma_{\gamma p}(S_{\gamma p}), \quad (6)$$

where S is the center of mass energy squared of the electron-proton system, and where $S_{\gamma p} = yS$ is its analog for the photon-proton system. We use for y_{min} and y_{max} the values given in Ref. [9], $y_{\text{min}} = 0.2$ and $y_{\text{max}} = 0.8$.

2.2 The factorized cross section

For our specific case, the inclusive cross section for dijet events with transverse energy greater than E_T , rapidity difference $\Delta\eta$, and energy flow less than Q_c in the intermediate region, of rapidity width Δy , can be written as follows [10, 11, 12, 13, 14]:

$$\begin{aligned} \frac{d\sigma_{ep}}{d\Delta\eta}(Q_c, S, E_T, \Delta y) &= \int_{y_{\min}}^{y_{\max}} dy F_{\gamma/e}(y) \\ &\times \left[\frac{d\sigma_{\gamma p}^{\text{dir}}}{d\Delta\eta}(Q_c, S_{\gamma p}, E_T, \Delta y) + \frac{d\sigma_{\gamma p}^{\text{res}}}{d\Delta\eta}(Q_c, S_{\gamma p}, E_T, \Delta y) \right]. \end{aligned} \quad (7)$$

Here $d\sigma_{\gamma p}^{\text{dir}}/d\Delta\eta$ and $d\sigma_{\gamma p}^{\text{res}}/d\Delta\eta$, are the direct and resolved contributions to the cross section respectively. In the former case the low-virtuality photon interacts directly with the parton from the proton, while in the latter, as mentioned above, it acts itself as a source of quarks and gluons, which then scatter off the partons from the proton. The two cross sections can be written in factorized form as [10, 11, 12, 13, 14]

$$\begin{aligned} \frac{d\sigma_{\gamma p}^{\text{dir}}}{d\Delta\eta}(Q_c, S_{\gamma p}, E_T, \Delta y) &= \sum_{f_p, f_1, f_2} \int_{R_{x_p}} dx_p \phi_{f_p/p}(x_p, -\hat{t}) \\ &\times \frac{d\hat{\sigma}^{(\gamma f)}}{d\Delta\eta}(Q_c, \hat{t}, \hat{s}, \eta_{JJ}, \Delta y, \alpha_s(\hat{t})), \end{aligned} \quad (8)$$

and

$$\begin{aligned} \frac{d\sigma_{\gamma p}^{\text{res}}}{d\Delta\eta}(Q_c, S_{\gamma p}, E_T, \Delta y) &= \sum_{f_\gamma, f_p, f_1, f_2} \int_{R_{x_\gamma}} dx_\gamma \int_{R_{x_p}} dx_p \phi_{f_\gamma/\gamma}(x_\gamma, -\hat{t}) \phi_{f_p/p}(x_p, -\hat{t}) \\ &\times \frac{d\hat{\sigma}^{(f)}}{d\Delta\eta}(Q_c, \hat{t}, \hat{s}, \eta_{JJ}, \Delta y, \alpha_s(\hat{t})). \end{aligned} \quad (9)$$

In these formulas $\phi_{f_\gamma/\gamma}$ and $\phi_{f_p/p}$ are parton distributions in the photon and proton respectively, evaluated at the scale $-\hat{t}$, the dijet momentum transfer, which is related to the partonic center of mass energy squared, \hat{s} , and the dijet rapidity difference, $\Delta\eta$, according to the formula $\hat{t} = -\frac{\hat{s}}{2} \left(1 - \tanh\left(\frac{\Delta\eta}{2}\right)\right)$. The integration regions for the partonic fractions x_p and x_γ are denoted by R_{x_p} and R_{x_γ} respectively. $d\hat{\sigma}^{(\gamma f)}/d\Delta\eta$ and $d\hat{\sigma}^{(f)}/d\Delta\eta$ are hard scattering functions, starting from the lowest order Born cross section. The index f (γf) denotes the partonic process $f_\gamma + f_p \rightarrow f_1 + f_2$ ($\gamma + f_p \rightarrow f_1 + f_2$). The detector geometry constrains the phase space for the dijet total pseudorapidity, $\eta_{JJ} = (\eta_{J1} + \eta_{J2})/2$, with $|\eta_{JJ}| < 0.75$ [9]. Similarly, the lower bound on the transverse energy of the jets, E_T , and the dijet pseudorapidity determine the phase space for the partonic center of mass energy squared \hat{s} , with $4E_T^2 \cosh^2\left(\frac{\Delta\eta}{2}\right) < \hat{s} < S_{\gamma p} \exp(2\eta_{JJ}) y E_e/E_p$.

2.3 Refactorization of the partonic scattering

In this section we will review some of the arguments already presented in Refs. [1, 20, 21, 22], to show how it is possible to perform a further factorization on the

partonic scattering functions, $d\hat{\sigma}^{(\gamma^f)}/d\Delta\eta$ and $d\hat{\sigma}^{(f)}/d\Delta\eta$, of Eqs. (8) and (9). The underlying argument is that in the partonic scattering the soft gluon emission decouples from the dynamics of the hard scattering, and can be approximated by an effective cross section, in which each of the partons is treated as a recoilless source of gluonic radiation. Formally, this is equivalent to replacing each parton with a path-ordered exponential of the gluon field (eikonal or Wilson line) in the proper representation of $SU(3)$, the fundamental representation 3 (3^*) for quarks (antiquarks), and the adjoint representation for gluons. In this way the hard amplitude is replaced by a sum of eikonal operators, $w_I(x)_{\{c_k\}}$, depending on color tensors c_I , which account for the color flow at the hard scattering, times short-distance coefficient functions. The effective dimensionless eikonal cross section (in the following f will refer to both direct and resolved processes) can be written as

$$\begin{aligned} \hat{\sigma}_{LI}^{(f,\text{eik})} \left(\frac{Q_c}{\mu}, \Delta y \right) &= \sum_{\xi} \theta(Q_c - E_c(\xi)) \\ &\times \langle 0 | \bar{T} \left[(w_L(0))_{\{b_i\}}^\dagger \right] | \xi \rangle \langle \xi | T \left[w_I(0)_{\{b_i\}} \right] | 0 \rangle, \end{aligned} \quad (10)$$

where we sum over all the final states subject to the constraint of having energy less than Q_c in the interjet region of rapidity Δy , while cutting off all the remaining integrals at the ultraviolet scale μ . This makes the eikonal cross section free from potential collinear singularities associated with gluon emission from the Wilson lines [8, 21, 22]. The Latin indexes I and L refer to the color structures of the amplitude and of its complex conjugate. At tree level, with no soft gluons, the above formula reduces to the square of eikonal vertices, with matrix elements given by traces of the color tensors in the amplitudes.

In these terms, the partonic scattering function can now be factorized into the product, in the space of color tensors, of a hard scattering matrix ¹, $H_{IL}^{(f)}$, accounting for the quanta of high virtuality exchanged in the scattering, and a soft matrix, $S_{LI}^{(f)}$,

$$\begin{aligned} \frac{d\hat{\sigma}_{\gamma p}^{(f)}}{d\Delta\eta} \left(Q_c, \hat{t}, \hat{s}, \eta_{JJ}, \Delta y, \alpha_s(\hat{t}) \right) &= \frac{\pi}{2\hat{s}} \left(2 \cosh^2 \left(\frac{\Delta\eta}{2} \right) \right)^{-1} \\ &\times H_{IL}^{(f)} \left(\sqrt{-\hat{t}}, \sqrt{\hat{s}}, \mu, \alpha_s(\mu^2) \right) S_{LI}^{(f)} \left(\Delta y, \frac{Q_c}{\mu} \right), \end{aligned} \quad (11)$$

where we follow the convention of the sum over repeated indices. This factorization holds to leading power in $\frac{\Lambda}{Q_c}$, with Λ the QCD scale parameter. We can identify a hard scale, $\sqrt{-\hat{t}}$, a soft scale, Q_c , and a new factorization scale, μ . The soft matrix, S_{LI} , precisely coincides with the gauge invariant eikonal cross section of Eq. (10),

$$S_{LI}^{(f)} \left(\frac{Q_c}{\mu}, \Delta y \right) = \hat{\sigma}_{LI}^{(f,\text{eik})} \left(\frac{Q_c}{\mu}, \Delta y \right). \quad (12)$$

¹The normalization of the dimensionless hard scattering matrix, $H_{IL}^{(f)}$, can be found in Eq. (68) below. It differs slightly from the one used in Ref. [1].

In general, corrections to the factorized expression in Eq. (11) are expected from three-jet final states, but, since the cost of adding an extra jet to the final state is at least one power of $\alpha_s(\hat{t})$, they will be suppressed.

2.4 Evolution of the soft matrix in color space

The left-hand side of the factorized expression, Eq. (11), is independent of μ . This means that the μ -dependence of the two matrices, $H_{IL}^{(f)}$ and $S_{LI}^{(f)}$, must cancel in the product. We thus derive for $S_{LI}^{(f)}$ the evolution equation [1]

$$\left(\mu \frac{\partial}{\partial \mu} + \beta(g) \frac{\partial}{\partial g} \right) S_{LI}^{(f)} = -(\Gamma_S^{(f)})_{LB}^\dagger S_{BI}^{(f)} - S_{LA}^{(f)} (\Gamma_S^{(f)})_{AI}, \quad (13)$$

where $\Gamma_S^{(f)}(\alpha_s)$ is a process-dependent soft anomalous dimension matrix. Solving this equation will enable us to resum all the leading logarithms of the soft scale Q_c . It is convenient to treat Eq. (13) in a basis which diagonalizes $\Gamma_S^{(f)}(\alpha_s)$. Following Ref. [22], we denote by Greek indexes the basis of the eigenvectors of $\Gamma_S^{(f)}(\alpha_s)$, $\{|e_\beta^{(f)}\rangle\}$, corresponding to the eigenvalues $\lambda_\beta^{(f)}$. We then transform Eq. (11) to this basis and solve the evolution equation (13) for $S^{(f)}$, by integrating with respect to μ between the soft scale Q_c and the hard scale $\sqrt{-\hat{t}}$, to get:

$$\begin{aligned} \frac{d\hat{\sigma}_{\gamma p}^{(f)}}{d\Delta\eta} (Q_c, \hat{s}, \hat{t}, \eta_{JJ}, \Delta y, \alpha_s(\hat{t})) &= \frac{\pi}{2\hat{s}} \left(2 \cosh^2 \left(\frac{\Delta\eta}{2} \right) \right)^{-1} \\ &\times \sum_{\alpha, \beta} H_{\beta\alpha}^{(f,1)} \left(\Delta y, \sqrt{\hat{s}}, \sqrt{-\hat{t}}, \alpha_s(\hat{t}) \right) S_{\alpha\beta}^{(f,0)}(\Delta y) \\ &\times \left[\ln \left(\frac{Q_c}{\Lambda} \right) \right]^{E_{\alpha\beta}^{(f)}} \left[\ln \left(\frac{\sqrt{-\hat{t}}}{\Lambda} \right) \right]^{-E_{\alpha\beta}^{(f)}}. \end{aligned} \quad (14)$$

The double differential cross section of Ref. [1], $d^2\hat{\sigma}_{\gamma p}^{(f)}/d\Delta\eta dQ_c$, giving the distribution of dijet events as a function of interjet radiation and rapidity interval, is obtained by differentiation with respect to Q_c . In the above formula the kinematical cuts on the jets require the minimum value of $\sqrt{-\hat{t}}$ to be exactly E_T ($E_T = 5\text{GeV}$ in Ref. [9]), still much larger than Λ . The exponents $E_{\alpha\beta}^{(f)}$ are given by

$$E_{\alpha\beta}^{(f)}(\Delta\eta, \Delta y) = \frac{2\pi}{\beta_1} \left[\hat{\lambda}_\alpha^{(f)*}(\Delta\eta, \Delta y) + \hat{\lambda}_\beta^{(f)}(\Delta\eta, \Delta y) \right], \quad (15)$$

where β_1 is the first coefficient in the expansion of the QCD β -function, $\beta_1 = \frac{11}{3}N_c - \frac{2}{3}n_f$, and where we define $\hat{\lambda}_\beta^{(f)}$ by $\lambda_\beta^{(f)} = \alpha_s \hat{\lambda}_\beta^{(f)} + \dots$. Observe that we have explicitly maintained a distinction between the dependence on $\Delta\eta$ and Δy , in spite of the fact that for this specific problem they are related through the identity in Eq. (4). In fact $\Delta\eta$ can be seen as a parameter of the hard scattering (related to the scattering

angle), whereas Δy , at fixed $\Delta\eta$, is a measure of the width of the interjet region and, as such, has a geometrical interpretation. The matrix $S_{\alpha\beta}^{(f,0)}$ in Eq. (14) is obtained by transforming to the new basis the zeroth order $S_{LI}^{(f,0)}$ of Eq. (11), which, as mentioned above, is just a set of color traces. The change of basis goes through the matrix $\left((R^{(f)})^{-1}\right)_{K\beta} \equiv \left(e_{\beta}^{(f)}\right)_K$, according to the formula [22]

$$S_{\alpha\beta}^{(f,0)} \equiv \left[\left((R^{(f)})^{-1}\right)^{\dagger}\right]_{\alpha M} S_{MN}^{(f,0)} \left((R^{(f)})^{-1}\right)_{N\beta}. \quad (16)$$

Analogously, we take for the $H_{IL}^{(f,1)}$'s the squares of the Born-level amplitudes, represented in the original color basis. In the diagonal basis, each hard matrix $H_{IL}^{(f,1)}$ becomes $H_{\beta\alpha}^{(f,1)}$, defined by

$$H_{\beta\alpha}^{(f,1)} = \left(R^{(f)}\right)_{\beta L} H_{LK}^{(f,1)} \left(R^{(f)\dagger}\right)_{K\alpha}. \quad (17)$$

Observe that $S^{(f,0)}$ and $H^{(f,1)}$ both acquire a Δy -dependence through the change of basis.

The relevant $\Delta\eta$ -dependence in the right hand side of Eq. (14) is contained in the exponents $E_{\alpha\beta}^{(f)}$, Eq. (15). We will see below that, for all the partonic processes, the real parts of the eigenvalues of $\Gamma_S^{(f)}(\alpha_s)$ in the exponents are positive definite functions, with boundary value $\text{Re}\left(\hat{\lambda}_{\beta}^{(f)}\right) = 0$ at $\Delta\eta = 2$ ($\Delta y = 0$). Then, since $Q_c < \sqrt{-\hat{t}}$, the last line in Eq. (14) acts as a suppression factor. Specifically, the eigenvalue with the biggest real part will drive the strongest suppression for the component of the scattering oriented along the direction of the corresponding eigenvector. As we shall see, most of the relevant information about the $\Delta\eta$ behavior of the cross section is derived from the properties of the soft anomalous dimension matrix $\Gamma_S^{(f)}(\alpha_s)$, which we will study in detail in Sec. 5.

3 The Gap Fraction

We will be interested in the evaluation of the gap fraction, defined as the ratio of the number of dijet events with a specified rapidity gap to the total number of dijet events. A gap event is usually identified experimentally by the lack of particle multiplicity in the interjet region [2, 9]. The multiplicity is determined from the number of calorimeter cells which measure energy deposition above a threshold, 300 MeV in the case of Ref. [9]. Therefore, the condition for a gap event is the absence of such cells (or clusters of cells) in the rapidity region between the jets. Our formulation of the problem, Eq. (7), is in terms of the total interjet flow, Q_c , of hadronic radiation, which is clearly related to particle multiplicity. In analogy with experiment, we introduce an energy threshold, Q_0 , which is different in principle from the experimental calorimeter threshold, and identify a gap event from the condition of interjet radiation less than Q_0 . From Eqs. (7), (8), (9) we see that the dependence on the interjet radiation is all in the partonic scattering, Eq. (14). Then, in order to get a dijet gap cross section,

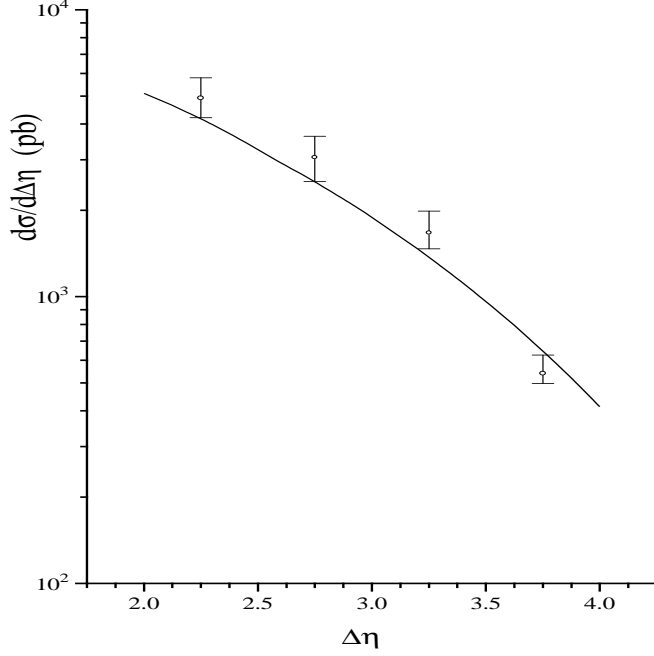


Figure 1: The overall dijet cross section compared with the experimental data of Ref. [9].

we just need to evaluate Eq. (14) at the threshold value Q_0 of the interjet energy flow Q_c ,

$$\begin{aligned}
\frac{d\hat{\sigma}_{\gamma p}^{(f),\text{gap}}}{d\Delta\eta} \left(Q_0, \hat{s}, \hat{t}, \eta_{JJ}, \Delta y, \alpha_s(\hat{t}) \right) &= \frac{\pi}{2\hat{s}} \left(2 \cosh^2 \left(\frac{\Delta\eta}{2} \right) \right)^{-1} \\
&\times \sum_{\alpha,\beta} H_{\beta\alpha}^{(f,1)} \left(\Delta y, \sqrt{\hat{s}}, \sqrt{-\hat{t}}, \alpha_s(\hat{t}) \right) S_{\alpha\beta}^{(f,0)}(\Delta y) \\
&\times \left[\ln \left(\frac{Q_0}{\Lambda} \right) \right]^{E_{\alpha\beta}^{(f)}} \left[\ln \left(\frac{\sqrt{-\hat{t}}}{\Lambda} \right) \right]^{-E_{\alpha\beta}^{(f)}}.
\end{aligned} \tag{18}$$

The denominator of the fraction is also obtained from Eq. (14), this time evaluated at the maximum value of Q_c , the hard scale $\sqrt{-\hat{t}}$. Values of Q_c above this scale would break the premise underlying the factorization in Eq. (11), since the emission into the interjet region would not be soft any more. By performing the substitution $Q_c = \sqrt{-\hat{t}}$ in Eq. (14) we find the full leading order partonic dijet cross section

$$\begin{aligned}
\frac{d\hat{\sigma}_{\gamma p}^{(f)}}{d\Delta\eta} \left(\hat{s}, \hat{t}, \eta_{JJ}, \Delta y, \alpha_s(\hat{t}) \right) &= \frac{\pi}{2\hat{s}} \left(2 \cosh^2 \left(\frac{\Delta\eta}{2} \right) \right)^{-1} \\
&\times H_{\beta\alpha}^{(f,1)} \left(\Delta y, \sqrt{\hat{s}}, \sqrt{-\hat{t}}, \alpha_s(\hat{t}) \right) S_{\alpha\beta}^{(f,0)}(\Delta y),
\end{aligned} \tag{19}$$

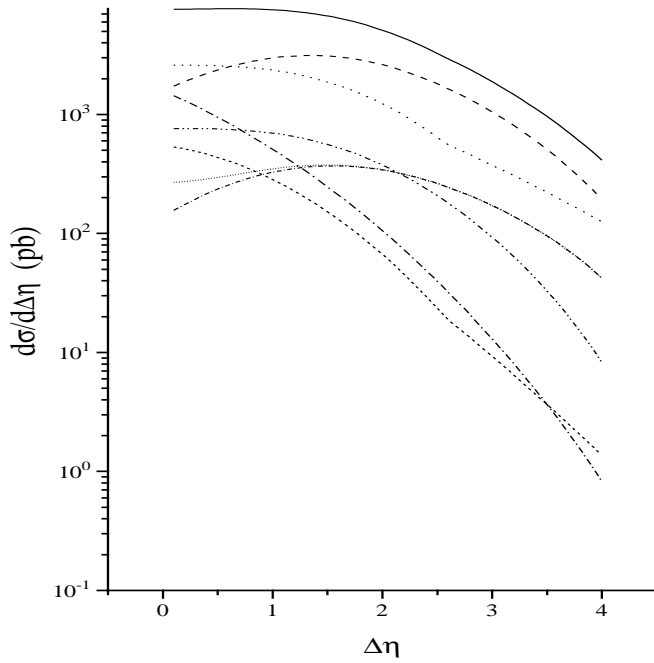


Figure 2: The contribution of the different partonic reactions to the dijet cross section. At $\Delta\eta = 0$ we can identify from top to bottom: the overall result (solid line); the contributions of: $\gamma + g \rightarrow q + \bar{q}$ (dotted line), $q + g \rightarrow q + g$ (dashed line), $q + g \rightarrow g + q$ (dot dashed line), $g + g \rightarrow g + g$ (double dot dashed line), $\gamma + q(\bar{q}) \rightarrow g + q(\bar{q})$ (short dashed line), $q + q \rightarrow q + q$ (short dotted line), $q + \bar{q} \rightarrow q + \bar{q}$ (short dot dashed line). Here the two reactions $q + g \rightarrow q + g$ and $q + g \rightarrow g + q$ differ from each other by the exchange of the Mandelstam invariants \hat{t} and \hat{u} (see Eqs. (69) and (70) in the Appendix).

where, from Eqs. (16) and (17), for each partonic process the trace identity $H_{\beta\alpha}^{(f,1)} S_{\alpha\beta}^{(f,0)} = H_{LI}^{(f,1)} S_{LI}^{(f,0)}$ holds, which is proportional to the leading order partonic cross section (see also Sec. 4 and Appendix A). After summing the gap and total cross sections over partonic subprocesses, as in Eqs. (8) and (9), the gap fraction has the form

$$f^{\text{gap}} = \frac{\frac{d\sigma_{ep}^{\text{gap}}}{d\Delta\eta}(Q_0, S, E_T, \Delta y)}{\frac{d\sigma_{ep}}{d\Delta\eta}(S, E_T, \Delta y)}. \quad (20)$$

In the numerical evaluation of the denominator of this fraction, we use, for each partonic reaction f in Eq. (19), the invariant S-matrix elements squared, and corresponding parton luminosities, $L^{(f)}$, summarized for completeness in Appendix A. We have used four quark flavors, $n_f = 4$, and have assumed flavor symmetry for the sea quarks. The numerical result we have found, shown in Fig. 1, is in reasonable agreement with the data points from Ref. [9]. Here it should be emphasized that, for the overall dijet cross section, and also, as we will see in Sec. 6, for the gap cross section,

corrections are expected from next-to-leading order contributions to the hard matrix [10, 11, 12, 14]. However, the gap fraction should not be too sensitive to them.

In Fig. 2 we show the partonic reactions most relevant to the overall cross section, evaluated on the full $\Delta\eta$ -range. For the $\Delta\eta$ -range of Ref. [9], $\Delta\eta > 2.0$, Fig. 3 clearly shows that it is sufficient to consider the contributions from the direct process, $\gamma + g \rightarrow q + \bar{q}$, the resolved gluon-initiated reactions, $q + g \rightarrow q + g$ and $g + g \rightarrow g + g$, and the quark processes, $q + \bar{q} \rightarrow q + \bar{q}$ and $q + q \rightarrow q + q$. These will also be the dominant contributions to the numerator of the fraction, which differs from the denominator only by the last two factors in Eq. (18), depending on the soft dynamics of each specific partonic reaction. The determination of the gap cross section will require an analysis of the partonic scattering in terms of color flow, to be found in the next Section, and the knowledge of the spectrum of the process-dependent soft anomalous dimension matrices, to be discussed in Sec. 5.

4 Lowest Order Hard and Soft Matrices in Color Space

In this section, we present the color decomposition of the hard scattering for the resolved partonic processes that have been shown above to give the dominant contribution to the dijet cross section in the $\Delta\eta$ region of interest. For each case, we will define a basis of color tensors, $\{|c^{(f)}_I\rangle\}$, and give, in this basis, the Born level hard matrix, $H_{LI}^{(f,1)}$, whose elements come from the squares of the color-decomposed tree amplitudes. We will also give the zeroth order soft matrix, $S_{LI}^{(f,0)}$, defined by the set of traces $S_{LI}^{(f,0)} = \text{Tr} \left[\left(c_L^{(f)} \right)^\dagger c_I^{(f)} \right]$. The knowledge of these matrices is not only crucial for the evaluation of Eqs. (18) and (19), but will be important for threshold resummation in jet production as well [23].

For the color tensors, following Ref. [22], we will find it convenient to use t -channel bases. In terms of momentum and color, we label the partonic process f according to $f_\gamma(l_A, r_A) + f_p(l_B, r_B) \rightarrow f_1(p_1, r_1) + f_2(p_2, r_2)$, where $\{l_A, r_A\}$, $\{l_B, r_B\}$ ($\{p_1, r_1\}$, $\{p_2, r_2\}$) are, respectively, the momenta and colors of the incoming (outgoing) partons. The hard matrix will be expressed in terms of the partonic Mandelstam invariants

$$\begin{aligned}\hat{s} &= (l_A + l_B)^2 \\ \hat{t} &= (l_A - p_1)^2 \\ \hat{u} &= (l_A - p_2)^2.\end{aligned}\tag{21}$$

It will also depend on the QCD running coupling evaluated at the hard scale, $(-\hat{t})^{1/2}$, according to the formula

$$\alpha_s(\hat{t}) = \frac{2\pi}{\beta_1 \ln\left((-\hat{t})^{1/2}/\Lambda\right)}.\tag{22}$$

For each process, it is straightforward to check that the color trace over the product of hard and soft matrices gives, as expected, the tree level invariant matrix element squared of Appendix A [24].

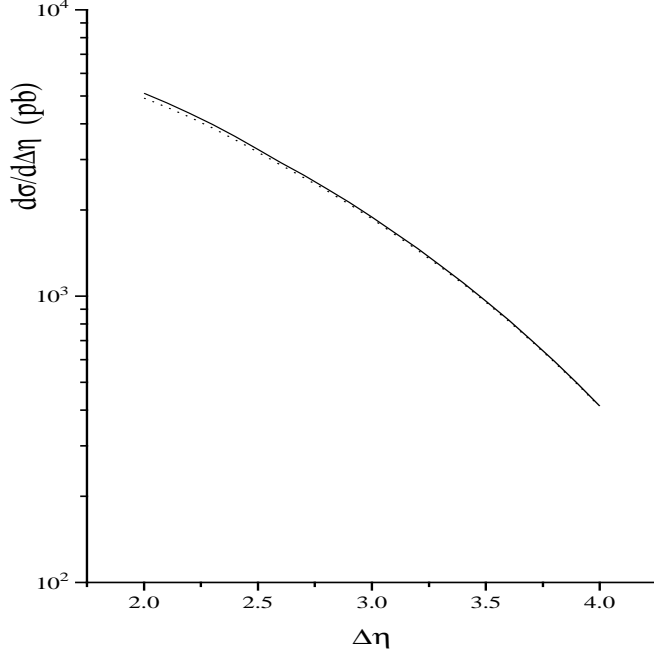


Figure 3: The dijet cross section (solid line) and the result obtained by dropping from Fig. 2 the contributions of the direct process $\gamma + q(\bar{q}) \rightarrow g + q(\bar{q})$, and of the resolved reaction $q + g \rightarrow g + q$ (dotted line).

4.1 Hard and soft matrix for $qg \rightarrow qg$

For the partonic process $q + g \rightarrow q + g$ we define the basis of color tensors [22]

$$\begin{aligned}
 c_1 &= \delta_{r_A, r_1} \delta_{r_B, r_2} \\
 c_2 &= d_{r_B r_2 c} (T_F^c)_{r_1 r_A} \\
 c_3 &= i f_{r_B r_2 c} (T_F^c)_{r_1 r_A},
 \end{aligned} \tag{23}$$

where c_1 is the t -channel singlet tensor, c_2 and c_3 the symmetric and antisymmetric octet respectively. Here and below, we suppress color indices on the c_I 's. In this basis, the Born level hard scattering can be described in color space by the matrix

$$H^{(1)} \left(\sqrt{-\hat{t}}, \sqrt{\hat{s}}, \alpha_s(\hat{t}) \right) = \frac{1}{48} \alpha_s^2(\hat{t}) \begin{pmatrix} \frac{1}{9}\chi_1 & \frac{1}{3}\chi_1 & \frac{2}{3}\chi_2 \\ \frac{1}{3}\chi_1 & \chi_1 & 2\chi_2 \\ \frac{2}{3}\chi_2 & 2\chi_2 & \chi_3 \end{pmatrix}, \tag{24}$$

with χ_1 , χ_2 and χ_3 functions of the partonic Mandelstam invariants:

$$\begin{aligned}
 \chi_1 &= 2 - \frac{\hat{t}^2}{\hat{s}\hat{u}} \\
 \chi_2 &= 1 - \frac{\hat{s}}{\hat{t}} - \frac{\hat{u}^2}{\hat{s}\hat{t}} - \frac{1}{2} \frac{\hat{t}^2}{\hat{s}\hat{u}}
 \end{aligned}$$

$$\chi_3 = 6 - 8 \frac{\hat{s}\hat{u}}{\hat{t}^2} - \frac{\hat{t}^2}{\hat{s}\hat{u}}. \quad (25)$$

It is easy to see that, in the limit of forward scattering ($\Delta\eta \rightarrow \infty$), the component of the hard matrix in the color direction of the antisymmetric octet becomes dominant, since it is $\mathcal{O}(\hat{t}^{-2})$.

The zeroth order soft matrix, on the other hand, is given by

$$S^{(0)} = \begin{pmatrix} N_c(N_c^2 - 1) & 0 & 0 \\ 0 & \frac{1}{2N_c}(N_c^2 - 4)(N_c^2 - 1) & 0 \\ 0 & 0 & \frac{1}{2}N_c(N_c^2 - 1) \end{pmatrix}, \quad (26)$$

where $N_c = 3$ is the number of colors.

4.2 Hard and soft matrix for $gg \rightarrow gg$

For this process, a suitable t -channel basis of color tensors has been defined in Ref. [22] to be:

$$\begin{aligned} c_1 &= \frac{i}{4} [f_{r_A r_B l} d_{r_1 r_2 l} - d_{r_A r_B l} f_{r_1 r_2 l}], \\ c_2 &= \frac{i}{4} [f_{r_A r_B l} d_{r_1 r_2 l} + d_{r_A r_B l} f_{r_1 r_2 l}], \\ c_3 &= \frac{i}{4} [f_{r_A r_1 l} d_{r_B r_2 l} + d_{r_A r_1 l} f_{r_B r_2 l}], \\ c_4 &= P_1(r_A, r_B; r_1, r_2) = \frac{1}{8} \delta_{r_A r_1} \delta_{r_B r_2}, \\ c_5 &= P_{8_S}(r_A, r_B; r_1, r_2) = \frac{3}{5} d_{r_A r_1 c} d_{r_B r_2 c}, \\ c_6 &= P_{8_A}(r_A, r_B; r_1, r_2) = \frac{1}{3} f_{r_A r_1 c} f_{r_B r_2 c}, \\ c_7 &= P_{10+\overline{10}}(r_A, r_B; r_1, r_2) = \frac{1}{2} (\delta_{r_A r_B} \delta_{r_1 r_2} - \delta_{r_A r_2} \delta_{r_B r_1}) \\ &\quad - \frac{1}{3} f_{r_A r_1 c} f_{r_B r_2 c}, \\ c_8 &= P_{27}(r_A, r_B; r_1, r_2) = \frac{1}{2} (\delta_{r_A r_B} \delta_{r_1 r_2} + \delta_{r_A r_2} \delta_{r_B r_1}) \\ &\quad - \frac{1}{8} \delta_{r_A r_1} \delta_{r_B r_2} - \frac{3}{5} d_{r_A r_1 c} d_{r_B r_2 c}. \end{aligned} \quad (27)$$

The last five elements of the basis are the t -channel $SU(3)$ projectors for the decomposition into irreducible representations of the direct product $8 \otimes 8$, which corresponds to the color content of a set of two gluons.

In this basis, the hard matrix has the block-diagonal structure

$$H^{(1)} \left(\sqrt{-\hat{t}}, \sqrt{\hat{s}}, \alpha_s(\hat{t}) \right) = \begin{pmatrix} 0_{3 \times 3} & 0_{3 \times 5} \\ 0_{5 \times 3} & H_{5 \times 5}^{(1)} \end{pmatrix}, \quad (28)$$

where the 5×5 submatrix $H_{5 \times 5}^{(1)}$ is given by

$$H_{5 \times 5}^{(1)} \left(\sqrt{-\hat{t}}, \sqrt{\hat{s}}, \alpha_s(\hat{t}) \right) = \frac{1}{16} \alpha_s^2(\hat{t}) \begin{pmatrix} 9\chi_1 & \frac{9}{2}\chi_1 & \frac{9}{2}\chi_2 & 0 & -3\chi_1 \\ \frac{9}{2}\chi_1 & \frac{9}{4}\chi_1 & \frac{9}{4}\chi_2 & 0 & -\frac{3}{2}\chi_1 \\ \frac{9}{2}\chi_2 & \frac{9}{4}\chi_2 & \chi_3 & 0 & -\frac{3}{2}\chi_2 \\ 0 & 0 & 0 & 0 & 0 \\ -3\chi_1 & -\frac{3}{2}\chi_1 & -\frac{3}{2}\chi_2 & 0 & \chi_1 \end{pmatrix}, \quad (29)$$

with χ_1 , χ_2 and χ_3 defined by

$$\begin{aligned} \chi_1 &= 1 - \frac{\hat{t}\hat{u}}{\hat{s}^2} - \frac{\hat{s}\hat{t}}{\hat{u}^2} + \frac{\hat{t}^2}{\hat{s}\hat{u}} \\ \chi_2 &= \frac{\hat{s}\hat{t}}{\hat{u}^2} - \frac{\hat{t}\hat{u}}{\hat{s}^2} + \frac{\hat{u}^2}{\hat{s}\hat{t}} - \frac{\hat{s}^2}{\hat{t}\hat{u}} \\ \chi_3 &= \frac{27}{4} - 9 \left(\frac{\hat{s}\hat{u}}{\hat{t}^2} + \frac{1\hat{t}\hat{u}}{4\hat{s}^2} + \frac{1\hat{s}\hat{t}}{4\hat{u}^2} \right) + \frac{9}{2} \left(\frac{\hat{u}^2}{\hat{s}\hat{t}} + \frac{\hat{s}^2}{\hat{t}\hat{u}} - \frac{1\hat{t}^2}{2\hat{s}\hat{u}} \right). \end{aligned} \quad (30)$$

Once again, it can be noticed that the component of the hard scattering in the color direction corresponding to the antisymmetric octet dominates in the forward limit.

For the zeroth order soft matrix, straightforward color traces with $N_c = 3$ colors give

$$S^{(0)} = \begin{pmatrix} -5 & 0 & 0 & 0 & 0 & 0 & 0 & 0 \\ 0 & -5 & 0 & 0 & 0 & 0 & 0 & 0 \\ 0 & 0 & -5 & 0 & 0 & 0 & 0 & 0 \\ 0 & 0 & 0 & 1 & 0 & 0 & 0 & 0 \\ 0 & 0 & 0 & 0 & 8 & 0 & 0 & 0 \\ 0 & 0 & 0 & 0 & 0 & 8 & 0 & 0 \\ 0 & 0 & 0 & 0 & 0 & 0 & 20 & 0 \\ 0 & 0 & 0 & 0 & 0 & 0 & 0 & 27 \end{pmatrix}. \quad (31)$$

We notice that the first three color tensors of the basis, Eq. (27), have negative eigenvalues, while the eigenvalues of the projectors count the number of color states belonging to each irreducible representation. In fact, c_1 , c_2 and c_3 of Eq. (27) decouple from the physical cross section. Eq. (28) supports this interpretation, since the components of the Born level hard scattering along these color directions vanish identically, reducing the dimensionality of the problem, in color space, from 8×8 to 5×5 . In principle, from Eqs. (16) and (17), the original dimensionality could be restored after the change from the color basis to the basis of the eigenvectors of the soft anomalous dimension matrix, Γ_S . We will show below that the structure of the specific Γ_S for $g + g \rightarrow g + g$ prevents this from happening.

4.3 Hard and soft matrix for $q\bar{q} \rightarrow q\bar{q}$ and $qq \rightarrow qq$

Both processes can be conveniently treated in the t -channel singlet-octet basis [22]

$$c_1 = \delta_{r_A, r_1} \delta_{r_B, r_2}$$

$$c_2 = -\frac{1}{2N_c}\delta_{r_A,r_1}\delta_{r_B,r_2} + \frac{1}{2}\delta_{r_A,r_B}\delta_{r_1,r_2}. \quad (32)$$

In color space, the hard matrix has the form

$$H^{(1)}\left(\sqrt{-\hat{t}}, \sqrt{\hat{s}}, \alpha_s(\hat{t})\right) = \frac{1}{9}\alpha_s^2(\hat{t}) \begin{pmatrix} \frac{32}{81}\chi_1 & \frac{1}{9}\chi_2 \\ \frac{1}{9}\chi_2 & \chi_3 \end{pmatrix}, \quad (33)$$

where, in the case of $q\bar{q} \rightarrow q\bar{q}$, χ_1 , χ_2 and χ_3 are defined by

$$\begin{aligned} \chi_1 &= \frac{\hat{t}^2 + \hat{u}^2}{\hat{s}^2} \\ \chi_2 &= 8\frac{\hat{u}^2}{\hat{s}\hat{t}} - \frac{8}{3}\frac{\hat{t}^2 + \hat{u}^2}{\hat{s}^2} \\ \chi_3 &= 2\frac{\hat{s}^2 + \hat{u}^2}{\hat{t}^2} + \frac{2}{9}\frac{\hat{t}^2 + \hat{u}^2}{\hat{s}^2} - \frac{4}{3}\frac{\hat{u}^2}{\hat{s}\hat{t}}, \end{aligned} \quad (34)$$

while in the case of $qq \rightarrow qq$, related to $q\bar{q} \rightarrow q\bar{q}$ by the crossing transformation $\hat{s} \leftrightarrow \hat{u}$, they are given by

$$\begin{aligned} \chi_1 &= \frac{\hat{t}^2 + \hat{s}^2}{\hat{u}^2} \\ \chi_2 &= 8\frac{\hat{s}^2}{\hat{t}\hat{u}} - \frac{8}{3}\frac{\hat{s}^2 + \hat{t}^2}{\hat{u}^2} \\ \chi_3 &= 2\frac{\hat{s}^2 + \hat{u}^2}{\hat{t}^2} + \frac{2}{9}\frac{\hat{s}^2 + \hat{t}^2}{\hat{u}^2} - \frac{4}{3}\frac{\hat{s}^2}{\hat{t}\hat{u}}. \end{aligned} \quad (35)$$

In both cases, for forward scattering, the component of the hard matrix along the color octet direction becomes dominant.

For the lowest order soft matrix, after the color trace, we find the common simple form [1]

$$S^{(0)} = \begin{pmatrix} N_c^2 & 0 \\ 0 & \frac{1}{4}(N_c^2 - 1) \end{pmatrix}. \quad (36)$$

5 The Soft Anomalous Dimension Matrix

In this section we shall describe how to compute the process-dependent soft anomalous dimension matrix, $\Gamma_S^{(f)}$ [8]. The μ -independence of the left hand side of Eq. (11) implies that the matrices $H_{IL}^{(f)}$ and $S_{LI}^{(f)}$ renormalize multiplicatively,

$$\begin{aligned} H_{IL}^{(f)(B)} &= \left(Z_S^{(f)-1}\right)_{IC} H_{CD}^{(f)} \left[(Z_S^{(f)\dagger})^{-1}\right]_{DL} \\ S_{LI}^{(f)(B)} &= (Z_S^{(f)\dagger})_{LB} S_{BA}^{(f)} Z_{S,AI}^{(f)}, \end{aligned} \quad (37)$$

where the superscript (B) identifies the bare quantities, and $Z_{S,CD}^{(f)}$ is a matrix of renormalization constants, describing the renormalization of the soft function, i. e. ,

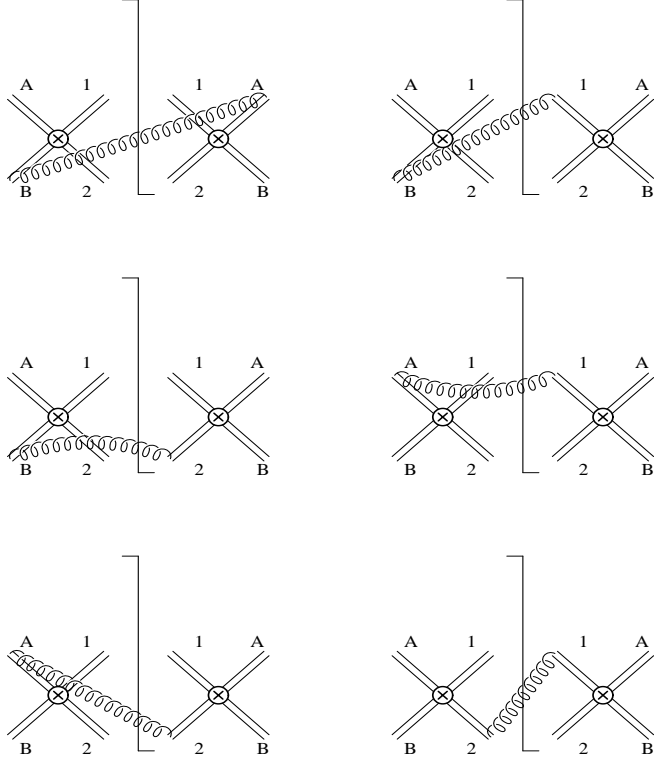


Figure 4: Real corrections to the eikonal scattering, Eq. (10). For brevity, we only show half of the contributing cut diagrams. The remaining ones can be obtained by hermitian conjugation of each of the above graphs, i. e. , by reflection with respect to the final state cut.

the eikonal scattering, Eq. (12). The one-loop anomalous dimension $\Gamma_S^{(f)}$ is obtained from the residue of the UV pole contained in the matrix $Z_S^{(f)}$,

$$\left(\Gamma_S^{(f)}\right)_{LI}(g) = -\frac{g}{2} \frac{\partial}{\partial g} \text{Res}_{\epsilon \rightarrow 0} \left(Z_S^{(f)}\right)_{LI}(g, \epsilon). \quad (38)$$

From Eq. (10) we see that the potential sources of UV divergences are the virtual vertex corrections to the eikonal color-dependent operators $w_I(x)_{\{c_k\}}$, and also the real corrections, when gluons are emitted into the forward region of the scattering, because the eikonal cross section, Eq. (10), is completely inclusive with respect to the amount of forward radiation.

The Feynman rules for the evaluation of eikonal diagrams have been presented in Ref. [22]. The necessary one-loop calculations are illustrated in Figs. 4-5: given the two color vertices c_I and c_L , corresponding to the hard amplitude and to its complex conjugate, we build the eikonal cross section from the product of the color-dependent eikonal operators, $w_I(x)_{\{c_k\}}$ and $\left(w_L(x)_{\{c_k\}}\right)^\dagger$, Eq. (10), and we compute the diagrams obtained by adding one extra real or virtual gluon, shown respectively in Fig. 4 and

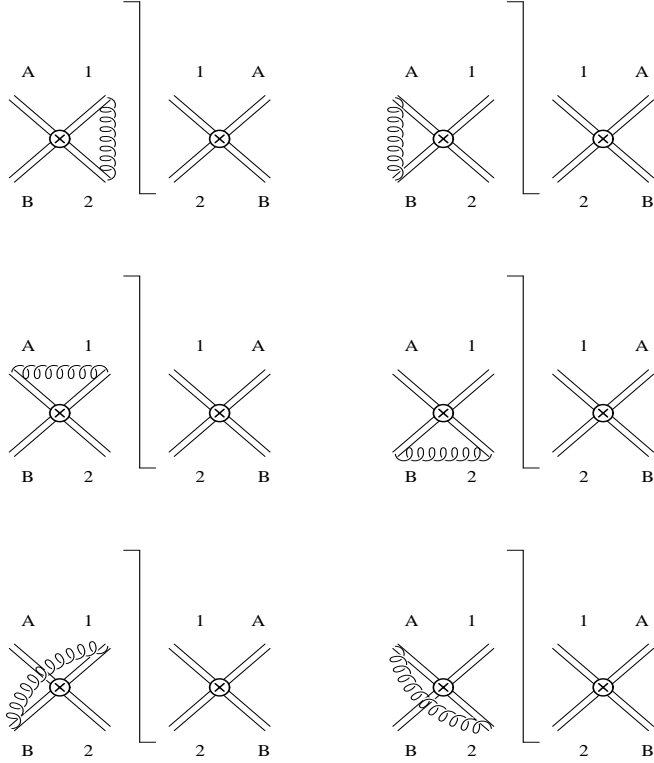


Figure 5: Virtual corrections to the eikonal scattering, Eq. (10). For brevity, we only show half of the contributing cut diagrams. The remaining ones can be obtained by hermitian conjugation of each of the above graphs, i. e. , by reflection with respect to the final state cut.

5. Working in Feynman gauge, the self-energy diagrams do not contribute, because they are proportional to the invariant mass of each lightlike eikonal line.

From the loop integration, it is easy to see that the UV divergences from the gluon emission diagrams and from the virtual diagrams with the gluon emitted and reabsorbed between an incoming and an outgoing eikonal line, are real. On the other hand, the coefficient of the UV pole from virtual diagrams with the gluon emitted and reabsorbed between two incoming or two outgoing eikonal lines, also have imaginary parts. Since the imaginary part of the soft anomalous dimension matrix comes only from virtual eikonal diagrams, it can be extracted directly from Ref. [22], where contributions to Γ_S are computed, for most partonic processes, from the virtual corrections to the eikonal operators $w_I(x)_{\{c_k\}}$. The real parts of the UV divergences coming, respectively, from virtual and real emission diagrams partially cancel in the sum, leaving a remainder which is a function of Δy , the width of the interjet rapidity region, where the gluon radiation is measured, and of the scattering-dependent parameter $\Delta\eta$.

We will now present, for each of the partonic processes relevant to the dijet cross

section, the result for $\Gamma_S^{(f)}$, and the analysis of its eigenvalues and eigenvectors, which we will relate to the behavior of the cross section, Eq. (14). For the direct reaction $\gamma + g \rightarrow q + \bar{q}$, which has only color octet content, $\Gamma_S^{(f)}$ will reduce to a function, related by crossing to the soft anomalous dimension computed in Ref. [25] for direct photon production.

We will see below, for all the resolved reactions, that the eigenvectors of Γ_S are mixed color states, and that their color composition is a function of the gap width only, through the ‘‘geometrical’’ parameter Δy . We have already pointed out in Eq. (4) that, in the experimental configuration of Ref. [9], $\Delta\eta$ fixes Δy , leaving us with only one independent parameter. We should emphasize, however, that for the case of the Tevatron rapidity gaps [1, 8], where the gap is taken fixed in the calorimeter detector, and is independent of the dynamics of the scattering, the eigenvectors have the same form as for this problem. Below, we will find it convenient to refer to the eigenvectors as ‘‘quasi-color’’ states (quasi-octet, quasi-singlet, and so on), identified by their behavior in the limit of asymptotically large gap regions, where they reduce to pure color states. We will discover that the eigenvalue with the smallest real part always corresponds to the quasi-singlet eigenvector, and we will show, from the discussion in Sec. 2.3, that the related component of the hard scattering is the only one to survive for large values of Δy .

5.1 Soft anomalous dimension for $qg \rightarrow qg$

In the basis of Eq. (23), the one-loop soft anomalous dimension matrix is

$$\Gamma_S(\Delta\eta, \Delta y) = \frac{\alpha_s}{2\pi} \begin{pmatrix} \rho_1 + \xi_1 & 0 & 2i\pi \\ 0 & \rho_1 & N_c i\pi \\ 4i\pi & \frac{N_c^2 - 4}{N_c} i\pi & \rho_1 \end{pmatrix}, \quad (39)$$

where the functions ρ_1 and ξ_1 are defined as follows:

$$\begin{aligned} \xi_1(\Delta y) &= N_c (i\pi - 2\Delta y), \\ \rho_1(\Delta\eta, \Delta y) &= N_c \left[2 \ln \left(\frac{\tanh(\frac{\Delta\eta}{2}) + \tanh(\frac{\Delta y}{2})}{\tanh(\frac{\Delta\eta}{2}) - \tanh(\frac{\Delta y}{2})} \right) \right] + i\pi \frac{2N_c^2 - 1}{N_c} \\ &\quad - \frac{N_c^2 + 1}{2N_c} \left[\ln \left(\frac{\tanh(\frac{\Delta\eta}{2}) + \tanh(\frac{\Delta y}{2})}{\tanh(\frac{\Delta\eta}{2}) - \tanh(\frac{\Delta y}{2})} \right) + \ln \left(\frac{1 - \tanh(\frac{\Delta y}{2})}{1 + \tanh(\frac{\Delta y}{2})} \right) \right]. \end{aligned} \quad (40)$$

While the first function depends only on the rapidity width of the interjet region, the second also depends on the hard scattering through $\Delta\eta$.

The eigenvalues of the above matrix are given by

$$\begin{aligned} \lambda_1(\Delta\eta, \Delta y) &= \frac{\alpha_s}{2\pi} \left[\frac{2\rho_1 + \xi_1}{3} + e^{\frac{2i\pi}{3}} (s_1 + s_2) \right] \\ \lambda_2(\Delta\eta, \Delta y) &= \frac{\alpha_s}{2\pi} \left[\frac{2\rho_1 + \xi_1}{3} + \left(e^{\frac{4i\pi}{3}} s_1 + s_2 \right) \right] \end{aligned}$$

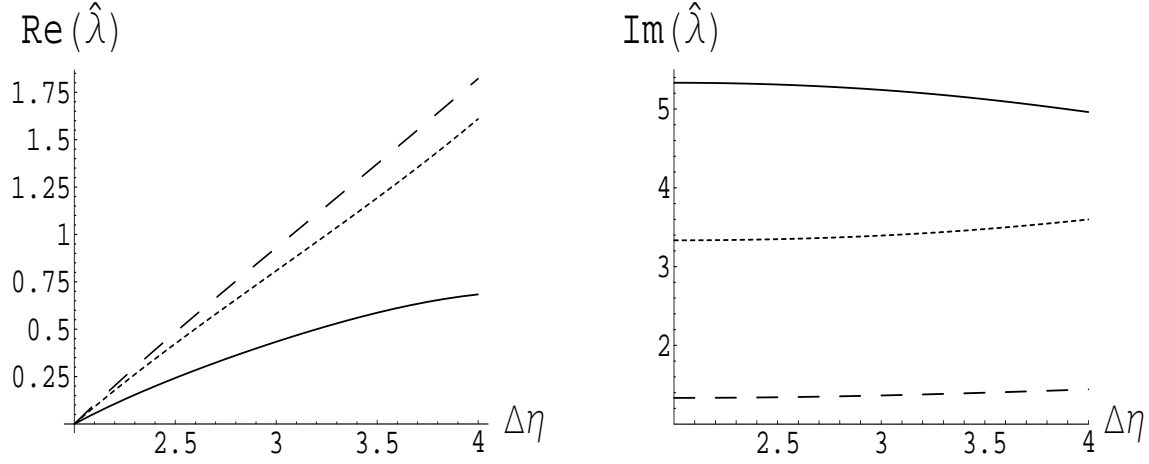


Figure 6: Plot of the real (left) and imaginary (right) part of the eigenvalues ($\hat{\lambda}_i = \lambda_i/\alpha_s$) of the soft anomalous dimension matrix for $q+g \rightarrow q+g$ scattering. The solid line identifies the quasi-singlet eigenvalue, $\hat{\lambda}_1$, the dashed and short dashed lines the two quasi-octets, $\hat{\lambda}_2$ and $\hat{\lambda}_3$.

$$\lambda_3(\Delta\eta, \Delta y) = \frac{\alpha_s}{2\pi} \left[\frac{2\rho_1 + \xi_1}{3} + \left(s_1 + e^{\frac{4i\pi}{3}} s_2 \right) \right], \quad (41)$$

where s_1 and s_2 , in the Δy range of Ref. [9]², $\Delta y < 2$, are the functions

$$s_1(\Delta y) \equiv \left[\frac{\xi_1^3}{27} + \frac{\pi^2}{3}(N_c^2 - 8)\xi_1 + \left(\frac{\pi^2}{27}(N_c^2 - 4)\xi_1^4 + \frac{2\pi^4}{27}\xi_1^2(N_c^4 - 28N_c^2 + 88) + \frac{\pi^6}{27}(N_c^2 + 4)^3 \right)^{\frac{1}{2}} \right]^{\frac{1}{3}}, \quad (42)$$

and

$$s_2(\Delta y) \equiv \left[\frac{\xi_1^3}{27} + \frac{\pi^2}{3}(N_c^2 - 8)\xi_1 - \left(\frac{\pi^2}{27}(N_c^2 - 4)\xi_1^4 + \frac{2\pi^4}{27}\xi_1^2(N_c^4 - 28N_c^2 + 88) + \frac{\pi^6}{27}(N_c^2 + 4)^3 \right)^{\frac{1}{2}} \right]^{\frac{1}{3}}. \quad (43)$$

The eigenvectors corresponding to the eigenvalues of Eq. (41) can be written in

²The definitions of s_1 and s_2 given in Eqs. (42) and (43) are valid for $\Delta y < 4\pi\frac{\sqrt{10}}{15}$, the branch point of the square root on the right hand side of Eqs. (42) and (43). For larger values of Δy , the square root picks the second branch definition. Consequently, s_1 and s_2 are switched.

unnormalized form as

$$\begin{aligned}
e_1 &= \begin{pmatrix} \frac{2i\pi}{4\Delta y - 2i\pi + e^{\frac{2i\pi}{3}}(s_1 + s_2)} \\ \frac{3i\pi}{-2\Delta y + i\pi + e^{\frac{2i\pi}{3}}(s_1 + s_2)} \\ 1 \end{pmatrix}, & e_2 &= \begin{pmatrix} \frac{2i\pi}{4\Delta y - 2i\pi + \left(e^{\frac{4i\pi}{3}} s_1 + s_2\right)} \\ \frac{3i\pi}{-2\Delta y + i\pi + \left(e^{\frac{4i\pi}{3}} s_1 + s_2\right)} \\ 1 \end{pmatrix} \\
e_3 &= \begin{pmatrix} \frac{2i\pi}{4\Delta y - 2i\pi + \left(s_1 + e^{\frac{4i\pi}{3}} s_2\right)} \\ \frac{3i\pi}{-2\Delta y + i\pi + \left(s_1 + e^{\frac{4i\pi}{3}} s_2\right)} \\ 1 \end{pmatrix}.
\end{aligned} \tag{44}$$

They depend only on the geometrical parameter Δy . It can be easily checked that in the limit $\Delta y \rightarrow \infty$ they become pure color states, e_1 a singlet, e_2 and e_3 antisymmetric and symmetric combinations of the two color octets in the basis, Eq. (23). However, for the values of Δy we are interested in, they are color-mixed states. Following Ref. [1], we will refer to e_1 as the quasi-singlet, and to e_2 and e_3 as the two quasi-octets. Numerical values of the real and imaginary parts of the eigenvalues are represented in Fig. 6. According to the discussion at the end of Sec. 2.4, the quasi-octet components of the hard scattering, for large values of Δy , will have strong suppression factors, compared to the quasi-singlet, because their real parts grow much faster. In fact, we will see in Sec. 6 that, in this situation, only the quasi-singlet component of the scattering survives.

5.2 Soft anomalous dimension for $gg \rightarrow gg$

We work in the basis of Eq. (27). The structure of the soft anomalous dimension matrix is block-diagonal:

$$\Gamma_S(\Delta\eta, \Delta y) = \begin{pmatrix} \Gamma_{3 \times 3} & 0_{3 \times 5} \\ 0_{5 \times 3} & \Gamma_{5 \times 5} \end{pmatrix}, \tag{45}$$

with the matrix $\Gamma_{3 \times 3}$ given by:

$$\Gamma_{3 \times 3} = \frac{\alpha_s}{2\pi} \begin{pmatrix} 3\rho_2 - 3i\pi & 0 & 0 \\ 0 & -3(\xi_2 - \rho_2) & 0 \\ 0 & 0 & 3\rho_2 + 3i\pi \end{pmatrix}, \tag{46}$$

and the matrix $\Gamma_{5 \times 5}$ given by:

$$\Gamma_{5 \times 5} = \frac{\alpha_s}{2\pi} \begin{pmatrix} 3\xi_2 + \rho_2 + 2i\pi & 0 & -12i\pi & 0 & 0 \\ 0 & 3\rho_2 & -3i\pi & -6i\pi & 0 \\ -\frac{3}{2}i\pi & -3i\pi & 3\rho_2 & 0 & -\frac{9}{2}i\pi \\ 0 & -\frac{12}{5}i\pi & 0 & -3(\xi_2 - \rho_2) & -\frac{18}{5}i\pi \\ 0 & 0 & -\frac{4}{3}i\pi & -\frac{8}{3}i\pi & 3\rho_2 - 5\xi_2 \end{pmatrix}. \tag{47}$$

The functions ξ_2 and ρ_2 are very similar to ξ_1 and ρ_1 of Eq. (40),

$$\xi_2(\Delta y) = i\pi - 2\Delta y, \quad (48)$$

$$\rho_2(\Delta\eta, \Delta y) = 2 \ln \left(\frac{\tanh(\frac{\Delta\eta}{2}) + \tanh(\frac{\Delta y}{2})}{\tanh(\frac{\Delta\eta}{2}) - \tanh(\frac{\Delta y}{2})} \right) + 3i\pi. \quad (49)$$

The eigenvalues of the matrix are

$$\begin{aligned} \lambda_1 &= \lambda_5 = 3 \frac{\alpha_s}{2\pi} (\rho_2 - i\pi) \\ \lambda_2 &= \lambda_4 = 3 \frac{\alpha_s}{2\pi} (\rho_2 - \xi_2) \\ \lambda_3 &= \lambda_6 = 3 \frac{\alpha_s}{2\pi} (\rho_2 + i\pi) \\ \lambda_7 &= \frac{\alpha_s}{2\pi} (3\rho_2 - \xi_2 - 4\eta_2) \\ \lambda_8 &= \frac{\alpha_s}{2\pi} (3\rho_2 - \xi_2 + 4\eta_2), \end{aligned} \quad (50)$$

where we have introduced the following function of the interjet rapidity:

$$\eta_2(\Delta y) = 2\sqrt{\Delta y^2 - i\pi\Delta y - \pi^2}. \quad (51)$$

Due to the block structure of the soft anomalous dimension matrix, the eigenvectors corresponding to the first three eigenvalues coincide with c_1 , c_2 and c_3 of Eq. (27), while the remaining eigenvectors have zero components along these color directions. Correspondingly, the structure of the matrix $R^{(f)^{-1}}$, and consequently $R^{(f)}$, of Eqs. (16) and (17), is block-diagonal,

$$R^{(f)^{-1}} = \begin{pmatrix} 1_{3 \times 3} & 0_{3 \times 5} \\ 0_{5 \times 3} & R^{(f)^{-1}}_{5 \times 5} \end{pmatrix}. \quad (52)$$

Referring to the discussion below Eq. (31), and to Eqs. (16) and (17), we see that the dimensionality of the hard scattering remains 5×5 after the change from the original basis to the basis of the eigenvectors of Γ_S , because the soft dynamics of the physical and unphysical color modes are completely decoupled. Here, once again, the eigenvectors depend only on the gap width Δy . Explicitly, we find

$$e_i = \begin{pmatrix} \delta_{i1} \\ \delta_{i2} \\ \delta_{i3} \\ 0^{(5)} \end{pmatrix}, \quad i = 1, 2, 3, \quad e_i = \begin{pmatrix} 0^{(3)} \\ e_i^{(5)} \end{pmatrix}, \quad i = 4 \dots 8. \quad (53)$$

For $e_4^{(5)}$, $e_5^{(5)}$ and $e_6^{(5)}$ we have the simple results

$$e_4^{(5)} = \begin{pmatrix} 0 \\ -\frac{3}{2} \\ 0 \\ -\frac{3}{4} - \frac{3i\Delta y}{2\pi} \\ 1 \end{pmatrix}, \quad e_5^{(5)} = \begin{pmatrix} -15 \\ \frac{15i}{4\pi} \left(\frac{2i\pi}{5} - 2\Delta y \right) \\ \frac{15i}{4\pi} (2i\pi - 2\Delta y) \\ 3 \\ 1 \end{pmatrix}, \quad e_6^{(5)} = \begin{pmatrix} -15 \\ 6 + \frac{15i}{2\pi} \Delta y \\ -\frac{15i}{2\pi} \Delta y \\ -3 \\ 1 \end{pmatrix}. \quad (54)$$

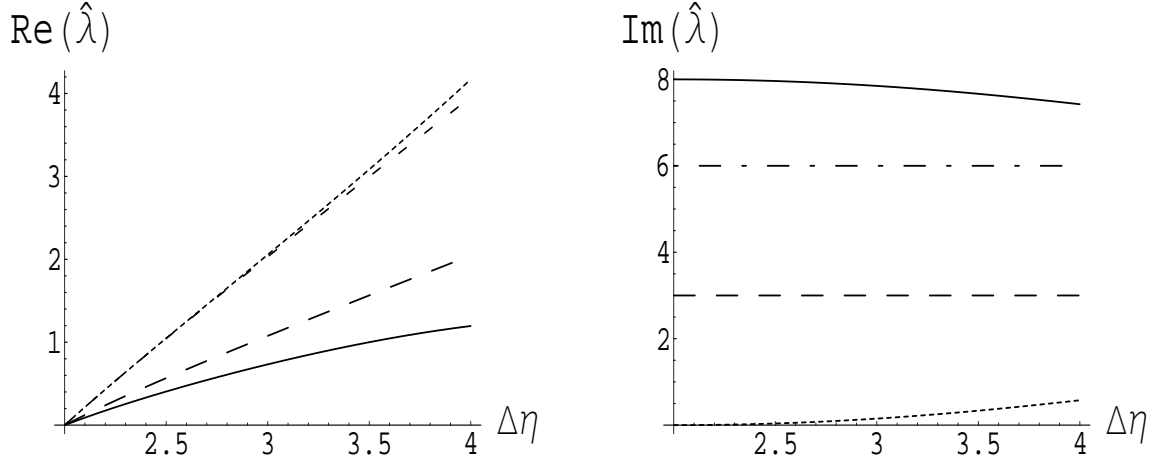


Figure 7: Plot of the real (left) and imaginary (right) part of the eigenvalues ($\hat{\lambda}_i = \lambda_i/\alpha_s$) of the soft anomalous dimension matrix for $g + g \rightarrow g + g$ scattering. In both plots the solid line identifies the quasi-singlet eigenvalue, $\hat{\lambda}_7$, and the dotted line the quasi-27, $\hat{\lambda}_8$. In the plot of the real parts the dashed line identifies the two degenerate quasi-octets, $\hat{\lambda}_5$ and $\hat{\lambda}_6$, and the short dashed line the quasi $10 + \overline{10}$. In the plot of the imaginary parts the dashed line corresponds to both the quasi-octet $\hat{\lambda}_5$ and the quasi $10 + \overline{10}$, whereas the dot dashed line identifies the other quasi-octet, $\hat{\lambda}_6$.

It is easy to see that for large interjet regions ($\Delta y \rightarrow \infty$) $e_4^{(5)}$ is oriented along the 10×10 color component, while $e_5^{(5)}$ and $e_6^{(5)}$ are respectively symmetric and antisymmetric combinations of the 8_S and 8_A color components. The last two eigenvectors have a more complicated analytic form:

$$\begin{aligned} e_7^{(5)} &= e_+^{(5)} \\ e_8^{(5)} &= e_-^{(5)}, \end{aligned} \quad (55)$$

with:

$$\begin{aligned} (e_{\pm}^{(5)})_1 &= \frac{27}{\mathcal{N}_{\pm}\pi^2} \left[32\Delta y^4 - 16i\Delta y^3 (4\pi \pm i\eta_2) - 4\pi\Delta y^2 (19\pi \pm 6i\eta_2) \right. \\ &\quad \left. + 4\pi^2 i\Delta y (11\pi \pm 5i\eta_2) + \pi^3 (13\pi \pm 6i\eta_2) \right] \\ (e_{\pm}^{(5)})_2 &= \frac{27}{\mathcal{N}_{\pm}} \left[-4\Delta y^2 - 2\Delta y (-2i\pi \pm \eta_2) + \pi (3\pi \pm i\eta_2) \right] \\ (e_{\pm}^{(5)})_3 &= \frac{9}{\mathcal{N}_{\pm}\pi} \left[24i\Delta y^3 + 12\Delta y^2 (3\pi \pm i\eta_2) + 2\pi\Delta y (\pm 6\eta_2 - 17i\pi) \right. \\ &\quad \left. - \pi^2 (11\pi \pm 7i\eta_2) \right] \\ (e_{\pm}^{(5)})_4 &= \frac{-9\pi}{\mathcal{N}_{\pm}} (2i\Delta y + \pi \pm 2i\eta_2) \\ (e_{\pm}^{(5)})_5 &= 1. \end{aligned} \quad (56)$$

In the denominators, the normalization \mathcal{N}_\pm is given by

$$\mathcal{N}_\pm = -28\Delta y^2 + 4i\Delta y(7\pi \pm i\eta_2) + \pi(31\pi \pm 2i\eta_2). \quad (57)$$

It is easily checked that $e_7^{(5)}$, in the limit of a very wide interjet region, reduces to a pure color singlet state, while $e_8^{(5)}$ points to the 27 color direction. Again, for typical values of Δy , these eigenvectors are not pure color states, but rather reflect mixing between the different color components of the hard scattering. From the eigenvalues of Eq. (50), plotted in Fig. 7, we can see, as already for $q + g \rightarrow q + g$, that the quasi-singlet component of the scattering, $e_7^{(5)}$, dominates the others in the limit of large gaps.

5.3 Soft anomalous dimension for $q\bar{q} \rightarrow q\bar{q}$

In the basis of Eq. (32), the soft anomalous dimension matrix is

$$\Gamma_S(\Delta\eta, \Delta y) = \frac{\alpha_s}{4\pi} \begin{pmatrix} \rho_0 + \xi_0 & -4\frac{C_F}{N_c}i\pi \\ -8i\pi & \rho_0 - \xi_0 \end{pmatrix}, \quad (58)$$

where the functions ξ_0 and ρ_0 are the analogs of those in Eqs. (40) and (49),

$$\begin{aligned} \xi_0(\Delta y) &= -2N_c\Delta y + 2i\pi\frac{N_c^2 - 2}{N_c}, \\ \rho_0(\Delta\eta, \Delta y) &= 2\frac{N_c^2 - 1}{N_c} \ln \left(\frac{\tanh\left(\frac{\Delta\eta}{2}\right) + \tanh\left(\frac{\Delta y}{2}\right)}{\tanh\left(\frac{\Delta\eta}{2}\right) - \tanh\left(\frac{\Delta y}{2}\right)} \right) \\ &\quad + \frac{2}{N_c}\Delta y - 2i\pi\frac{N_c^2 - 2}{N_c}. \end{aligned} \quad (59)$$

In particular, ρ_0 , which depends on the scattering angle, differs slightly from the corresponding function computed in Ref. [1] for the Tevatron gaps, because of the different underlying kinematics. On the other hand ξ_0 , depending only on the geometry, through Δy , is identical. The two eigenvalues are

$$\begin{aligned} \lambda_1(\Delta\eta, \Delta y) &= \frac{\alpha_s}{2\pi} \left[\frac{1}{2}\rho_0 - \frac{1}{2\sqrt{N_c}}\sqrt{N_c\xi_0^2 - 32C_F\pi^2} \right] \\ \lambda_2(\Delta\eta, \Delta y) &= \frac{\alpha_s}{2\pi} \left[\frac{1}{2}\rho_0 + \frac{1}{2\sqrt{N_c}}\sqrt{N_c\xi_0^2 - 32C_F\pi^2} \right], \end{aligned} \quad (60)$$

corresponding to the eigenvectors

$$\begin{aligned} e_1 &= \begin{pmatrix} 1 \\ \frac{8\pi}{i} \left(\xi_0 - \frac{1}{\sqrt{N_c}}\sqrt{N_c(\xi_0(\Delta y))^2 - 32C_F\pi^2} \right)^{-1} \end{pmatrix} \\ e_2 &= \begin{pmatrix} \frac{i}{8\pi} \left(\xi_0 + \frac{1}{\sqrt{N_c}}\sqrt{N_c(\xi_0(\Delta y))^2 - 32C_F\pi^2} \right) \\ 1 \end{pmatrix}, \end{aligned} \quad (61)$$

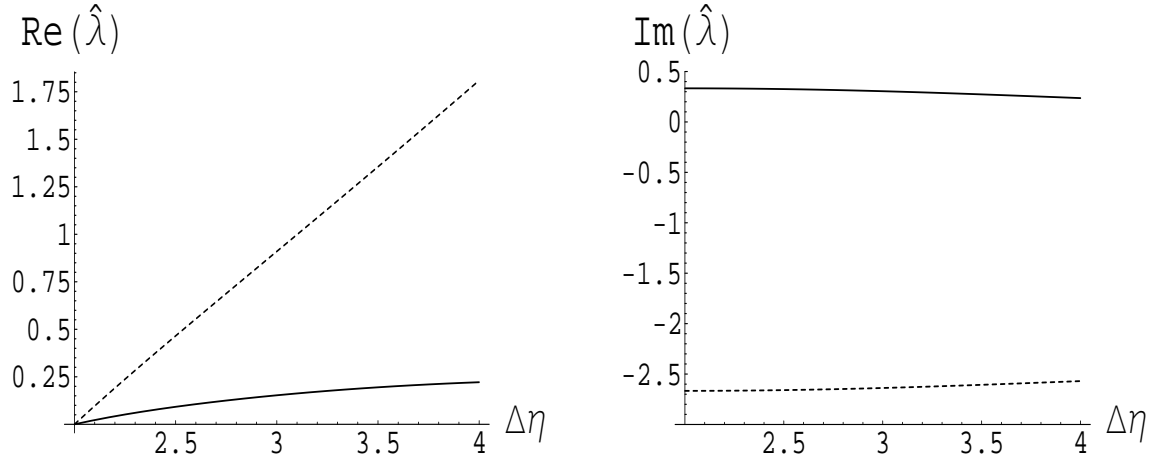


Figure 8: Plot of the real (left) and imaginary (right) part of the eigenvalues ($\hat{\lambda}_i = \lambda_i/\alpha_s$) of the soft anomalous dimension matrix for $q + \bar{q} \rightarrow q + \bar{q}$ scattering. The solid line identifies the quasi-singlet eigenvalue, $\hat{\lambda}_1$, the short dashed line the quasi-octet, $\hat{\lambda}_2$.

which coincide precisely with the ones given in Ref. [1], since they depend only on the geometric parameter Δy . In the limit of an asymptotically large gap, e_1 becomes a pure color singlet vector, while e_2 orients itself along the octet direction. Referring to e_1 and e_2 as quasi-singlet and quasi-octet, and looking at the behavior of the real parts of the eigenvalues, Fig. 8, we can predict that, also for this partonic process, the quasi-singlet component of the scattering in Eq. (14) will dominate the quasi-octet in the large gap limit.

5.4 Soft anomalous dimension for $qq \rightarrow qq$

In the basis of Eq. (32), the soft anomalous dimension matrix is

$$\Gamma_S(\Delta\eta, \Delta y) = \frac{\alpha_s}{4\pi} \begin{pmatrix} \rho'_0 + \xi'_0 - \frac{4i\pi}{N_c} & 4\frac{C_F}{N_c}i\pi \\ 8i\pi & \rho'_0 - \xi'_0 - \frac{4i\pi}{N_c} \end{pmatrix}, \quad (62)$$

where the functions ρ'_0 and ξ'_0 are:

$$\begin{aligned} \xi'_0(\Delta y) &= -2N_c\Delta y + \frac{4i\pi}{N_c}, \\ \rho'_0(\Delta\eta, \Delta y) &= 2\frac{N_c^2 - 1}{N_c} \left[\ln \left(\frac{\tanh\left(\frac{\Delta\eta}{2}\right) + \tanh\left(\frac{\Delta y}{2}\right)}{\tanh\left(\frac{\Delta\eta}{2}\right) - \tanh\left(\frac{\Delta y}{2}\right)} \right) + 2i\pi \right] + \frac{2}{N_c}\Delta y. \end{aligned} \quad (63)$$

The two eigenvalues are:

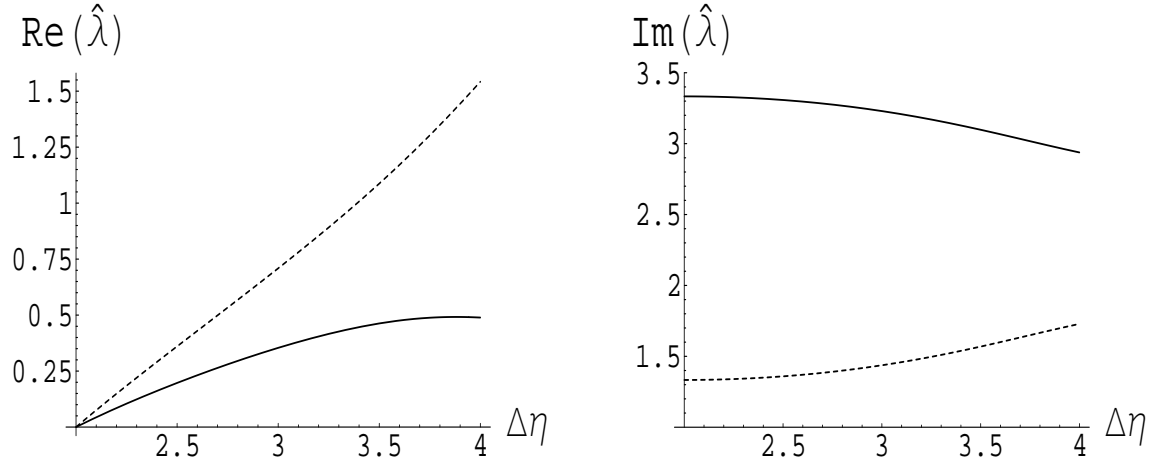


Figure 9: Plot of the real (left) and imaginary (right) part of the eigenvalues ($\hat{\lambda}_i = \lambda_i/\alpha_s$) of the soft anomalous dimension matrix for $q+q \rightarrow q+q$ scattering. The solid line identifies the quasi-singlet eigenvalue, $\hat{\lambda}_1$, the short dashed line the quasi-octet, $\hat{\lambda}_2$.

$$\begin{aligned} \lambda_1(\Delta\eta, \Delta y) &= \frac{\alpha_s}{2\pi} \left[\frac{1}{2}\rho'_0 - \frac{1}{2\sqrt{N_c}} \sqrt{N_c \xi_0'^2 - 32\pi^2 C_F} - \frac{2i\pi}{N_c} \right] \\ \lambda_2(\Delta\eta, \Delta y) &= \frac{\alpha_s}{2\pi} \left[\frac{1}{2}\rho'_0 + \frac{1}{2\sqrt{N_c}} \sqrt{N_c \xi_0'^2 - 32\pi^2 C_F} - \frac{2i\pi}{N_c} \right], \end{aligned} \quad (64)$$

which correspond to the eigenvectors:

$$\begin{aligned} e_1 &= \begin{pmatrix} \frac{4\pi C_F}{iN_c} \left(\xi'_0 + \frac{1}{\sqrt{N_c}} \sqrt{\xi_0'^2 - 32\pi^2 C_F} \right)^{-1} \\ 1 \end{pmatrix} \\ e_2 &= \begin{pmatrix} 1 \\ \frac{iN_c}{4\pi C_F} \left(\xi'_0 - \frac{1}{\sqrt{N_c}} \sqrt{\xi_0'^2 - 32\pi^2 C_F} \right) \end{pmatrix}. \end{aligned} \quad (65)$$

Notice the similarity with the process $q\bar{q} \rightarrow q\bar{q}$. We can again identify in e_1 the quasi-singlet, and in e_2 the quasi-octet. For large gaps, the quasi-octet component of the scattering will be strongly suppressed with respect to the quasi-singlet, because the real part of the corresponding eigenvalue grows much faster with $\Delta\eta$, as graphically shown in Fig. 9.

5.5 Soft anomalous dimension for $\gamma g \rightarrow q\bar{q}$

For the direct process $\gamma g \rightarrow q\bar{q}$, which, from Fig. 2, gives the second largest contribution to the denominator of the fraction, after the partonic reaction $qg \rightarrow qg$, there is only one possible color flow at the hard scattering. Thus, the soft anomalous

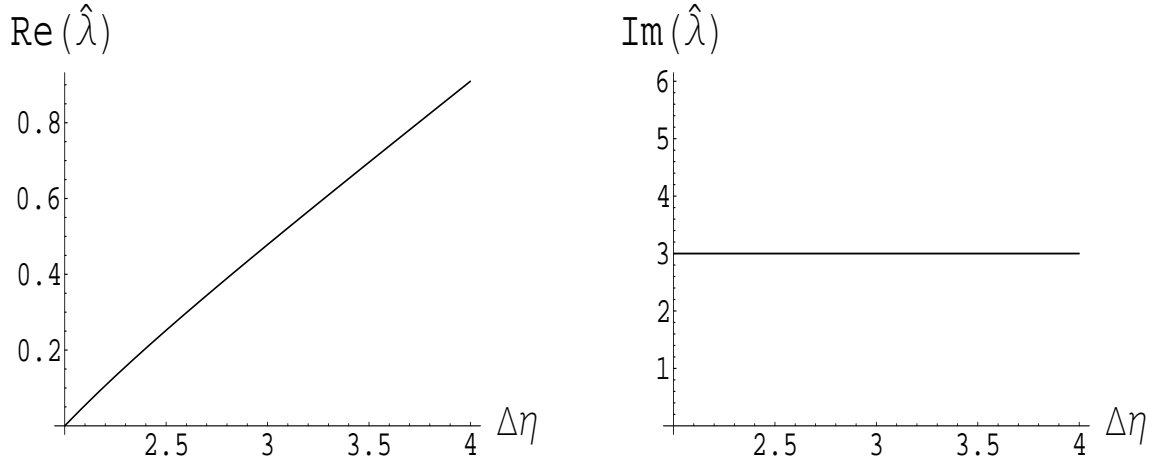


Figure 10: Plot of the real (left) and imaginary (right) part of the soft anomalous dimension for $\gamma + g \rightarrow q + \bar{q}$ scattering.

dimension reduces to a function, given by

$$\Gamma_S(\Delta\eta, \Delta y) = \frac{\alpha_s}{2\pi} \left[C_F \ln \left(\frac{\tanh\left(\frac{\Delta\eta}{2}\right) + \tanh\left(\frac{\Delta y}{2}\right)}{\tanh\left(\frac{\Delta\eta}{2}\right) - \tanh\left(\frac{\Delta y}{2}\right)} \right) + 2i\pi C_A \right], \quad (66)$$

whose real and imaginary ³ parts are plotted in Fig. 10. We see that the real part of Γ_S grows faster with $\Delta\eta$ than the real parts of the quasi-singlet eigenvalues for all the resolved processes, apart from $gg \rightarrow gg$, Figs. 6 - 9. In fact, we will see in the next section that the corresponding contribution to the gap cross section will have a fast decay rate.

6 Numerical Results and Discussion

From the previous two sections, we have all the tools necessary for the evaluation of the partonic gap cross section, Eq. (18), which we convolute with the parton distributions and with the photon distribution in the electron, according to Eq. (7), to get the full gap cross section. The necessary numerical integrals have been performed with the routine VEGAS. We have used the CTEQ4L parton distribution set [26] for the proton, and the GRV-G LO set [27] for the photon. For the interjet energy threshold Q_0 , which in our approach defines the gap event (see Sec. 3), we have considered several different values, from $Q_0 = 350\text{MeV}$ up to $Q_0 = 1050\text{MeV}$, and we have evaluated the related gap cross section as a function of the pseudorapidity difference between the jets, $\Delta\eta$. Figs. 11a,b show our results for the gap cross section and the corresponding gap fraction. Both quantities increase with increasing Q_0 , simply

³The imaginary part of Eq. (66) can be extracted directly from Ref. [25].

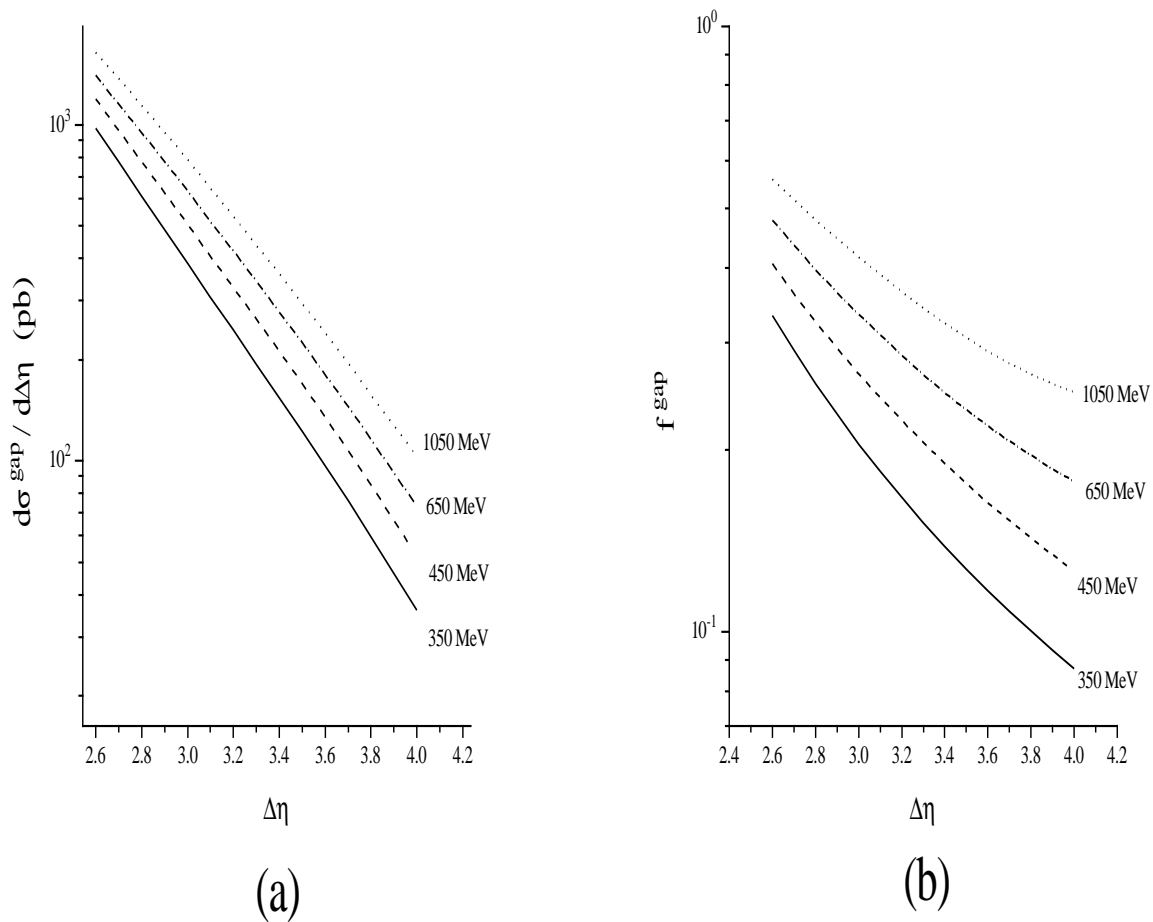


Figure 11: The gap cross section (a) and fraction (b) at different values of the energy threshold Q_0 identifying the gap (see Eq. (18)).

because a stronger limitation on interjet radiation leads to a stronger suppression of the result. For the most forward configuration of the dijet analyzed in Ref. [9], $\Delta\eta = 3.75$, the gap fraction, Fig. 11b, varies from about 10% at $Q_0 = 350\text{MeV}$ to about 25% at $Q_0 = 1050\text{MeV}$. One may ask, for both the gap cross section and the gap fraction, whether any of the plots in Figs. 11a,b fits the experimental data of Ref. [9], for which, as discussed in Sec. 3, the gap event is identified in a related, but different way. With the choice $Q_0 = 350\text{MeV}$ for the interjet energy, we obtain a good match, as shown in Fig. 12a,b. Observe that, in this situation, Q_0 is not much larger than Λ in Eq. (18). Results in this region, at the boundary with non-perturbative QCD, can be considered as smooth extrapolations of perturbative QCD resummation.

In Fig. 13, the analog of Fig. 3d of Ref. [9], we show again our gap fraction at $Q_0 = 350\text{MeV}$, from Eqs. (18) and (19), and compare it with the result of a two parameter fit to the expression

$$f^{\text{fit}}(\alpha, \beta, \Delta\eta) = C(\alpha, \beta) e^{\alpha\Delta\eta} + \beta. \quad (67)$$

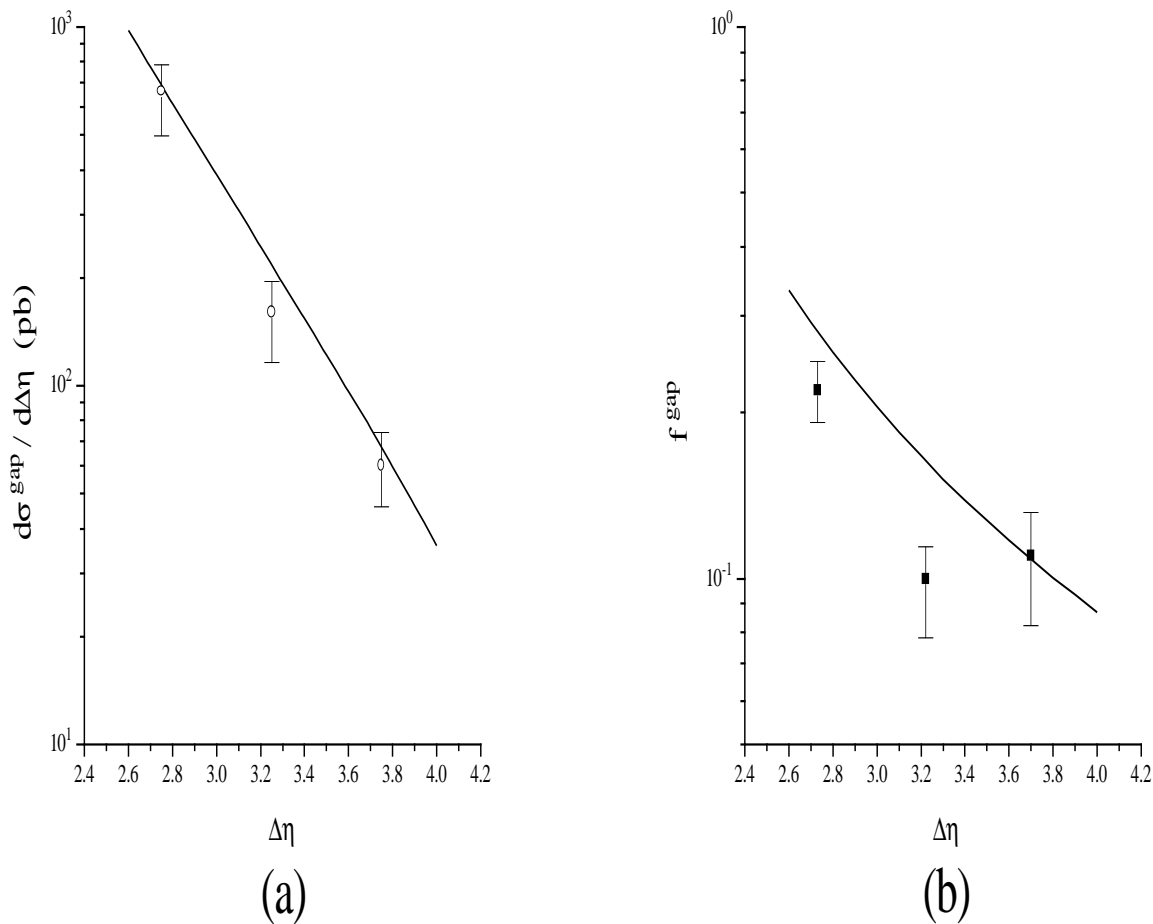


Figure 12: The gap cross section (a) and fraction (b), for the gap identified by the energy threshold $Q_0 = 350\text{MeV}$, compared with the data of Ref. [9].

as done in Ref. [9]. We find $\alpha = -2.1$ and $\beta = 8.3\%$, in good agreement with the values of Ref. [9]: $\alpha = -2.7 \pm 0.3$ and $\beta = (7 \pm 2)\%$. Here, in analogy with Ref. [9], we have imposed the constraint $f^{\text{fit}} = 1$ at $\Delta\eta = 2$, meaning that the gap cross section has to reduce to the full dijet cross section in the absence of a gap. Notice that this information is not encoded in Eq. (18), because the last two factors on the right hand side do not reduce exactly to unity for $\Delta\eta = 2$. This can be seen from Eq. (15) and from the eigenvalues of the soft anomalous dimension matrices, Figs. 6-10. In the limit $\Delta\eta \rightarrow 2$, the real parts of the eigenvalues vanish, but the imaginary parts do not, causing a slight suppression in the mixed terms, ($\beta \neq \gamma$), of the hard scattering matrix in Eq. (18). The validity of our formula for the gap cross section, Eq. (18), is restricted to interjet rapidity widths Δy neither too small, nor too large. We will limit ourselves to the $\Delta\eta$ range $2.6 < \Delta\eta < 4.0$.

The reasons for these restrictions are as follows. Our expression in Eq. (18) is the result of the resummation of logarithms of the soft interjet energy, $\alpha_s^n(-\hat{t}) \ln^n(Q_0/\sqrt{-\hat{t}})$, which are assumed to be the only large, perturbatively dangerous quantities in the

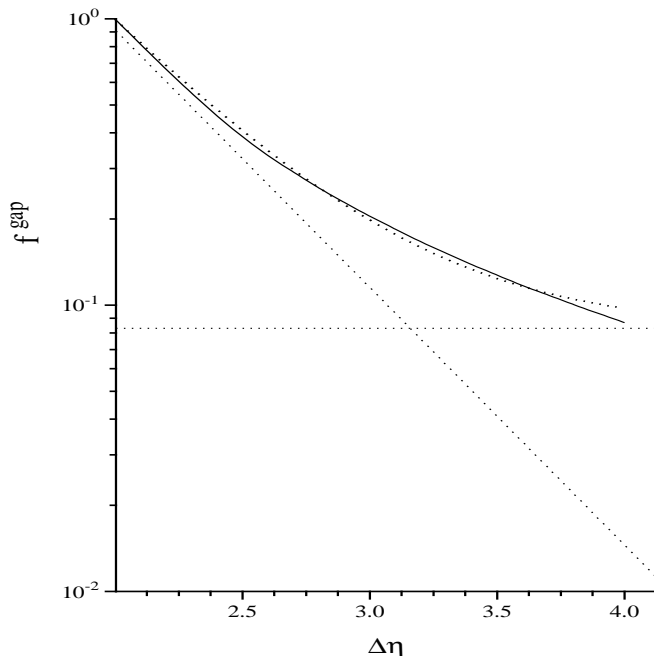


Figure 13: Analog of Fig. 3d of Ref. [9]. The gap fraction of Fig. 12 (solid line) is redisplayed and compared with the result of a fit to an exponential plus a constant.

problem. When $\Delta y \rightarrow 0$, the gap closes and the cross section becomes inclusive. More specifically, logarithms of $\sqrt{-\hat{t}}$ would be suppressed by powers of Δy . Analogously, when $\Delta y \rightarrow \infty$ (i. e. , $\Delta\eta \rightarrow \infty$), terms of the form $\alpha_s^n(-\hat{t})(\Delta y)^n$, coming from the eigenvalues of the $\Gamma_S^{(f)}$'s, are large at each order in perturbation theory, and we need further resummations. We should also emphasize that the limit $\Delta\eta \rightarrow \infty$ corresponds to the Regge region of the scattering, when \hat{s} becomes large at fixed momentum transfer, \hat{t} . Resummation in the Regge limit organizes logarithms of the form $\alpha_s^n \ln^n(\hat{s}/(-\hat{t}))$, coming from the BFKL ladders of gluons [6]. For double logarithmic terms like $\alpha_s^n \ln^n(\hat{s}/(-\hat{t})) \ln^n(Q_0/\sqrt{-\hat{t}})$, which occur in Reggeized color octet exchange, both BFKL resummation and our method give the same result.

Note that the suppression we find here is not double logarithmic in Q_0 [28]. Rather, it comes from the exponentiation of single “soft” logarithms only, as shown in Eq. (13). The underlying physical reason is that a soft gluon emitted into the interjet region can never become collinear to either of the forward partons from which the jets originate.

Finally, in Figs. 14-17 we show the contributions to the gap cross section, Eq. (18) at $Q_0 = 350\text{MeV}$, from the different partonic processes studied in Sec. 5. In each case we give the full result and its decomposition into quasi-color components. We see that, as anticipated in Sec. 5, the quasi-singlet components, in all cases, give almost the whole gap cross section at large values of $\Delta\eta$. It then becomes clear that

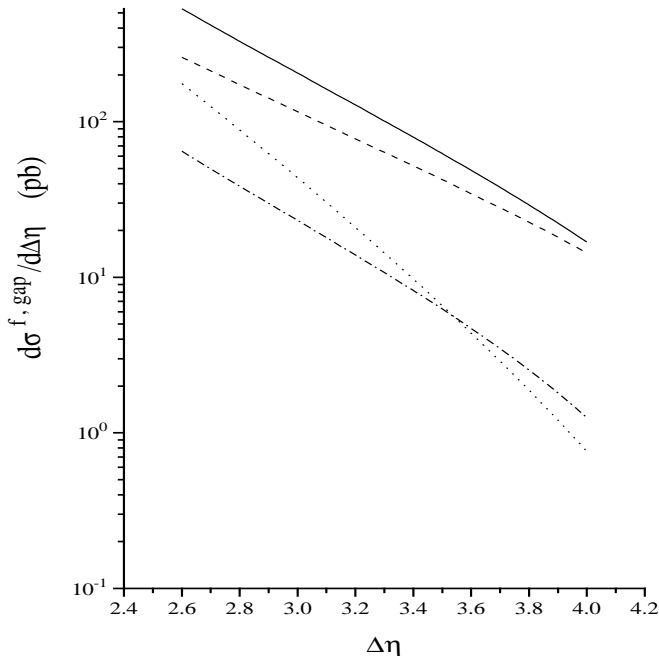


Figure 14: Overall contribution to the gap cross section from $qg \rightarrow qg$ scattering (solid line). Contribution from the quasi-singlet component (dashed) and from the two quasi-octet components (dotted and dot dashed).

the parameter $\beta = 8.3\%$, extracted from the fit, Eq. (67), can be associated with the asymptotic quasi-singlet fraction. From Figs. 6-9 we see that at high $\Delta\eta$ the real parts of the quasi-singlet eigenvalues are ordered, from the lowest value of $q\bar{q} \rightarrow q\bar{q}$ scattering, through the intermediate values of processes $qg \rightarrow qg$ and $qq \rightarrow qq$, up to the largest value of $gg \rightarrow gg$ scattering. In Figs. 14-17, the decay slopes of the quasi-singlet components of the corresponding contributions to the gap cross section reflect the same ordering property, as a consequence of Eq. (14). This observation indicates that gaps tend to be more easily formed with scattered quarks and antiquarks than with gluons [5].

7 Conclusions

In this paper, we have shown that it is possible to analyze the dijet rapidity gap events from photoproduction, observed at HERA, by introducing an energy-dependent definition of the gap, as already done in Ref. [1] for the Tevatron events. The result we have found is perturbative, as the ordering of the different scales in Eq. (14) shows, with $\Lambda < Q_c < \sqrt{-\hat{t}}$. The experimental behavior of the gap fraction is approximately reproduced by fixing the threshold of interjet energy, which defines the gap, at $Q_0 = 350\text{MeV}$. Our result also predicts how gap fractions increase with Q_0 . We

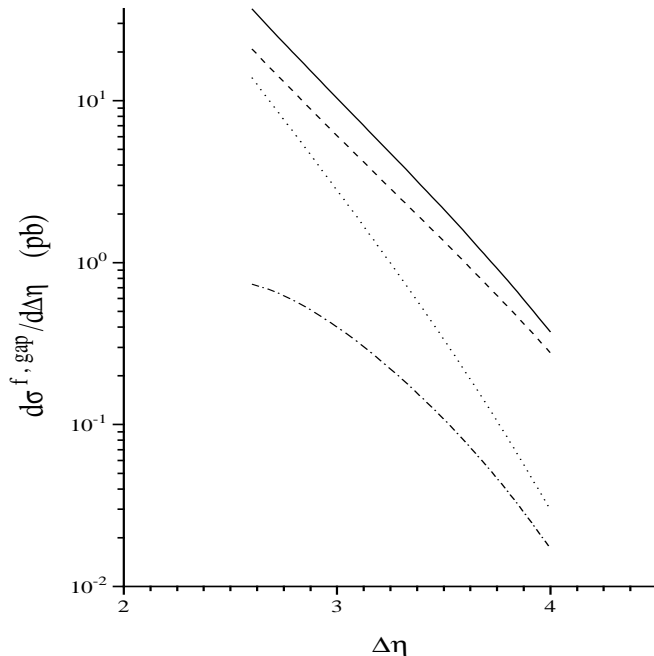


Figure 15: Overall contribution to the gap cross section from $gg \rightarrow gg$ scattering (solid line). Contribution from the quasi-singlet component (dashed) and from the two quasi-octet components (dotted and dot dashed). The contributions of the quasi- $10 \times \overline{10}$ and of the quasi-27 component are not exhibited, because they are too small.

conjecture that in photoproduction non-perturbative “survival” effects from the interactions of spectator partons, which can give rise to interjet multiplicity [17], should be reduced with respect to the case of $p\bar{p}$ scattering, because there is only one incoming hadron. The experimental determination of the double differential cross section $d^2\sigma_{ep}/d\Delta\eta dQ_c$, (and related fraction), Eq. (18), for different values of the interjet energy flow identifying the gap, as in Fig. 11, would offer a significant test of the perturbative dynamics of QCD radiation.

Acknowledgments

I would like to express my gratitude to Prof. George Sterman, for many conversations and insights, and for all his help. I am indebted to Brian Harris and Jack Smith for their valuable advice in the implementation of the numerical integrations. Finally I would like to thank Alan White, Jim Whitmore, and the other participants of the Theory Institute on Deep-Inelastic Diffraction (Argonne National Lab, September 14th - 16th, 1998), where the early stages of this work were presented, for useful discussions. This work was supported in part by the National Science Foundation, grant PHY9722101.

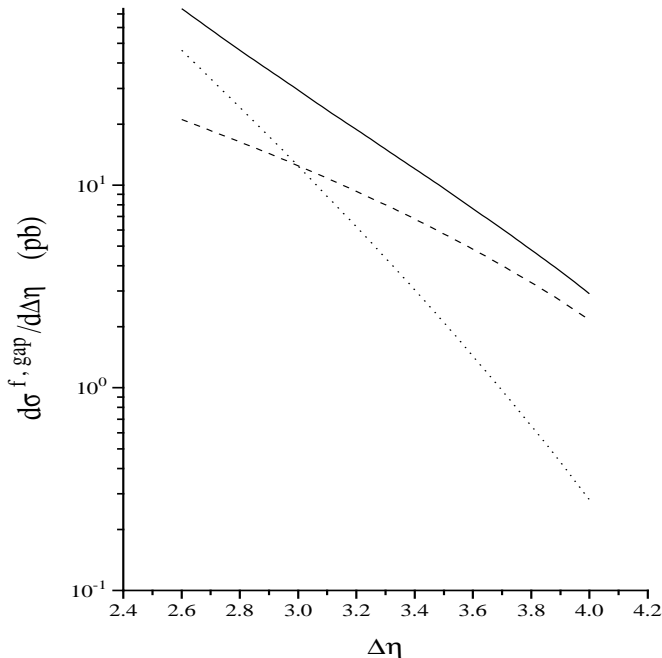


Figure 16: Overall contribution to the gap cross section from $q\bar{q} \rightarrow q\bar{q}$ scattering (solid line). Contribution from the quasi-singlet component (dashed) and from the quasi-octet component (dotted).

A The Denominator of the Gap Fraction: Partonic Cross Sections and Parton Luminosities

In this Appendix we will summarize for completeness the Born cross sections, and corresponding parton luminosities, $L^{(f)}$, for all the partonic processes contributing to the denominator of the gap fraction, Eq. (19). We will consider for the quarks four active flavors, $n_f = 4$, and assume flavor symmetry. Correspondingly, the quark luminosities will be expressed as functions of the proton valence distributions, $\phi_{u/p}$ and $\phi_{d/p}$, and of the sea distributions for both the proton and the photon, respectively $\phi_{\text{sea}/p}$ and $\phi_{\text{sea}/\gamma}$. The analytic cross sections will always be of the form

$$\begin{aligned} \frac{d\hat{\sigma}^{(f)}}{d\Delta\eta} &= \left(2 \cosh^2\left(\frac{\Delta\eta}{2}\right)\right)^{-1} \alpha_s^2(\hat{t}) \left(\frac{\pi}{2\hat{s}}\right) |\mathcal{M}^{(f)}(\hat{s}, \hat{t}, \hat{u})|^2 \\ &= \frac{\pi}{2\hat{s}} \left(2 \cosh^2\left(\frac{\Delta\eta}{2}\right)\right)^{-1} H_{IL}^{(f)}\left(\sqrt{-\hat{t}}, \sqrt{\hat{s}}, \mu, \alpha_s(\mu^2)\right) S_{LI}^{(f)}\left(\Delta y, \frac{Q_c}{\mu}\right), \end{aligned} \quad (68)$$

where, in both equalities, the first factor is the Jacobian $[d\cos(\hat{\theta})/d\Delta\eta]$, and the rest is the partonic cross section $d\hat{\sigma}^{(f)}/d\cos(\hat{\theta})$. The second equality defines the normalization of the hard scattering matrix in Eq. (11). In the list below, we will specify the invariant matrix elements squared, $|\mathcal{M}^{(f)}(\hat{s}, \hat{t}, \hat{u})|^2$ [14, 24].

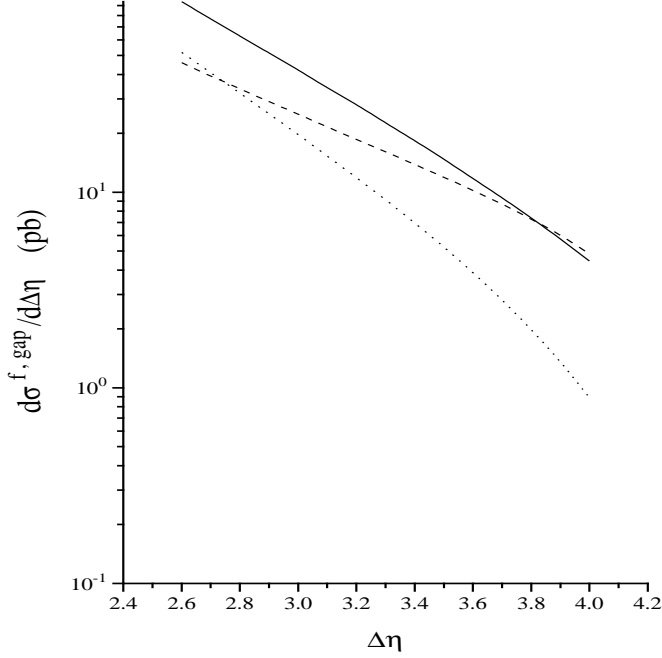


Figure 17: Overall contribution to the gap cross section from $qq \rightarrow qq$ scattering (solid line). Contribution from the quasi-singlet component (dashed) and from the quasi-octet component (dotted). Negative interference terms [1], corresponding to $\beta \neq \gamma$ in Eq. (18), are not exhibited separately.

- Processes $q(\bar{q})g \rightarrow q(\bar{q})g, gq(\bar{q}) \rightarrow gq(\bar{q})$:

$$\begin{aligned}
 L^{(f)} &= \phi_{g/\gamma} \left(\phi_{u/p} + \phi_{d/p} + 6\phi_{\text{sea}/p} \right) + 8\phi_{\text{sea}/\gamma} \phi_{g/p} \\
 |\mathcal{M}^{(f)}(\hat{s}, \hat{t}, \hat{u})|^2 &= \frac{\hat{u}^2 + \hat{s}^2}{\hat{t}^2} - \frac{4}{9} \frac{\hat{s}^2 + \hat{u}^2}{\hat{s}\hat{u}}.
 \end{aligned} \tag{69}$$

- Processes $q(\bar{q})g \rightarrow gq(\bar{q}), gq(\bar{q}) \rightarrow q(\bar{q})g$ (observe that they differ from the processes of Eq. (69) by the exchange of particles 1 and 2 in Eq. (21), and, correspondingly, of the Mandelstam invariants \hat{t} and \hat{u}):

$$\begin{aligned}
 L^{(f)} &= \phi_{g/\gamma} \left(\phi_{u/p} + \phi_{d/p} + 6\phi_{\text{sea}/p} \right) + 8\phi_{\text{sea}/\gamma} \phi_{g/p} \\
 |\mathcal{M}^{(f)}(\hat{s}, \hat{t}, \hat{u})|^2 &= \frac{\hat{t}^2 + \hat{s}^2}{\hat{u}^2} - \frac{4}{9} \frac{\hat{s}^2 + \hat{t}^2}{\hat{s}\hat{t}}.
 \end{aligned} \tag{70}$$

- Process $gg \rightarrow gg$:

$$\begin{aligned}
 L^{(f)} &= \phi_{g/\gamma} \phi_{g/p} \\
 |\mathcal{M}^{(f)}(\hat{s}, \hat{t}, \hat{u})|^2 &= \frac{9}{2} \left(3 - \frac{\hat{s}\hat{u}}{\hat{t}^2} + \frac{\hat{t}\hat{u}}{\hat{s}^2} + \frac{\hat{s}\hat{t}}{\hat{u}^2} \right).
 \end{aligned} \tag{71}$$

- Process $qq \rightarrow qq$:

$$\begin{aligned} L^{(f)} &= \phi_{\text{sea}/\gamma} \left(\phi_{u/p} + \phi_{d/p} + 6\phi_{\text{sea}/p} \right) \\ |\mathcal{M}^{(f)}(\hat{s}, \hat{t}, \hat{u})|^2 &= \frac{4}{9} \frac{\hat{s}^2 + \hat{u}^2}{\hat{t}^2} + \frac{4}{9} \frac{\hat{s}^2 + \hat{t}^2}{\hat{u}^2} - \frac{8}{27} \frac{\hat{s}^2}{\hat{t}\hat{u}}. \end{aligned} \quad (72)$$

- Process $qq' \rightarrow qq'$:

$$\begin{aligned} L^{(f)} &= 3\phi_{\text{sea}/\gamma} \left(\phi_{u/p} + \phi_{d/p} + 6\phi_{\text{sea}/p} \right) \\ |\mathcal{M}^{(f)}(\hat{s}, \hat{t}, \hat{u})|^2 &= \frac{4}{9} \frac{\hat{s}^2 + \hat{u}^2}{\hat{t}^2}. \end{aligned} \quad (73)$$

- Process $qq' \rightarrow q'q$:

$$\begin{aligned} L^{(f)} &= 3\phi_{\text{sea}/\gamma} \left(\phi_{u/p} + \phi_{d/p} + 6\phi_{\text{sea}/p} \right) \\ |\mathcal{M}^{(f)}(\hat{s}, \hat{t}, \hat{u})|^2 &= \frac{4}{9} \frac{\hat{s}^2 + \hat{t}^2}{\hat{u}^2}. \end{aligned} \quad (74)$$

- Processes $q\bar{q} \rightarrow q\bar{q}$, $\bar{q}q \rightarrow \bar{q}q$:

$$\begin{aligned} L^{(f)} &= \phi_{\text{sea}/\gamma} \left(\phi_{u/p} + \phi_{d/p} + 6\phi_{\text{sea}/p} \right) \\ |\mathcal{M}^{(f)}(\hat{s}, \hat{t}, \hat{u})|^2 &= \frac{4}{9} \frac{\hat{s}^2 + \hat{u}^2}{\hat{t}^2} + \frac{4}{9} \frac{\hat{t}^2 + \hat{u}^2}{\hat{s}^2} - \frac{8}{27} \frac{\hat{u}^2}{\hat{s}\hat{t}}. \end{aligned} \quad (75)$$

- Processes $q\bar{q}' \rightarrow q\bar{q}'$, $\bar{q}q' \rightarrow \bar{q}q'$:

$$\begin{aligned} L^{(f)} &= 3\phi_{\text{sea}/\gamma} \left(\phi_{u/p} + \phi_{d/p} + 6\phi_{\text{sea}/p} \right) \\ |\mathcal{M}^{(f)}(\hat{s}, \hat{t}, \hat{u})|^2 &= \frac{4}{9} \frac{\hat{s}^2 + \hat{u}^2}{\hat{t}^2}. \end{aligned} \quad (76)$$

- Processes $q\bar{q} \rightarrow q'\bar{q}'$, $\bar{q}q \rightarrow \bar{q}'q'$:

$$\begin{aligned} L^{(f)} &= 3\phi_{\text{sea}/\gamma} \left(\phi_{u/p} + \phi_{d/p} + 6\phi_{\text{sea}/p} \right) \\ |\mathcal{M}^{(f)}(\hat{s}, \hat{t}, \hat{u})|^2 &= \frac{4}{9} \frac{\hat{t}^2 + \hat{u}^2}{\hat{s}^2}. \end{aligned} \quad (77)$$

- Processes $q\bar{q} \rightarrow \bar{q}q$, $\bar{q}q \rightarrow q\bar{q}$:

$$\begin{aligned} L^{(f)} &= \phi_{\text{sea}/\gamma} \left(\phi_{u/p} + \phi_{d/p} + 6\phi_{\text{sea}/p} \right) \\ |\mathcal{M}^{(f)}(\hat{s}, \hat{t}, \hat{u})|^2 &= \frac{4}{9} \frac{\hat{s}^2 + \hat{t}^2}{\hat{u}^2} + \frac{4}{9} \frac{\hat{t}^2 + \hat{u}^2}{\hat{s}^2} - \frac{8}{27} \frac{\hat{t}^2}{\hat{s}\hat{u}}. \end{aligned} \quad (78)$$

- Processes $q\bar{q}' \rightarrow \bar{q}'q$, $\bar{q}q' \rightarrow q'\bar{q}$:

$$\begin{aligned} L^{(f)} &= 3\phi_{\text{sea}/\gamma} \left(\phi_{u/p} + \phi_{d/p} + 6\phi_{\text{sea}/p} \right) \\ |\mathcal{M}^{(f)}(\hat{s}, \hat{t}, \hat{u})|^2 &= \frac{4}{9} \frac{\hat{s}^2 + \hat{t}^2}{\hat{u}^2}. \end{aligned} \quad (79)$$

- Processes $q\bar{q} \rightarrow \bar{q}'q'$, $\bar{q}q \rightarrow q'\bar{q}'$:

$$\begin{aligned} L^{(f)} &= 3\phi_{\text{sea}/\gamma} (\phi_{u/p} + \phi_{d/p} + 6\phi_{\text{sea}/p}) \\ |\mathcal{M}^{(f)}(\hat{s}, \hat{t}, \hat{u})|^2 &= \frac{4}{9} \frac{\hat{t}^2 + \hat{u}^2}{\hat{s}^2}. \end{aligned} \quad (80)$$

- Processes $q\bar{q} \rightarrow gg$, $\bar{q}q \rightarrow gg$

$$\begin{aligned} L^{(f)} &= \phi_{\text{sea}/\gamma} (\phi_{u/p} + \phi_{d/p} + 6\phi_{\text{sea}/p}) \\ |\mathcal{M}^{(f)}(\hat{s}, \hat{t}, \hat{u})|^2 &= -\frac{8}{3} \frac{\hat{t}^2 + \hat{u}^2}{\hat{s}^2} + \frac{32}{27} \frac{\hat{t}^2 + \hat{u}^2}{\hat{t}\hat{u}}. \end{aligned} \quad (81)$$

- Processes $gg \rightarrow q\bar{q}$, $gg \rightarrow \bar{q}q$

$$\begin{aligned} L^{(f)} &= \phi_{g/\gamma} \phi_{g/p} \\ |\mathcal{M}^{(f)}(\hat{s}, \hat{t}, \hat{u})|^2 &= -\frac{3}{8} \frac{\hat{t}^2 + \hat{u}^2}{\hat{s}^2} + \frac{1}{6} \frac{\hat{t}^2 + \hat{u}^2}{\hat{t}\hat{u}}. \end{aligned} \quad (82)$$

- Processes $\gamma g \rightarrow q\bar{q}$, $\gamma g \rightarrow \bar{q}q$

$$\begin{aligned} L^{(f)} &= 2\phi_{g/p} \\ |\mathcal{M}^{(f)}(\hat{s}, \hat{t}, \hat{u})|^2 &= \frac{10}{9} \frac{\alpha_{\text{em}}}{\alpha_s} \left(\frac{\hat{u}}{\hat{t}} + \frac{\hat{t}}{\hat{u}} \right). \end{aligned} \quad (83)$$

- Process $\gamma q(\bar{q}) \rightarrow q(\bar{q})g$,

$$\begin{aligned} L^{(f)} &= \frac{4}{9}\phi_{u/p} + \frac{1}{9}\phi_{d/p} + \frac{15}{9}\phi_{\text{sea}/p} \\ |\mathcal{M}^{(f)}(\hat{s}, \hat{t}, \hat{u})|^2 &= \frac{\alpha_{\text{em}}}{\alpha_s} \left(\frac{-\hat{u}}{\hat{s}} + \frac{\hat{s}}{-\hat{u}} \right). \end{aligned} \quad (84)$$

References

- [1] G. Oderda and G. Sterman, Phys. Rev. Lett. **81**, 3591 (1998).
- [2] S. Abachi *et al.* (D0 Collaboration), Phys. Rev. Lett. **76**, 734 (1996); F. Abe *et al.* (CDF Collaboration), Phys. Rev. Lett. **80**, 1156 (1998); Phys. Rev. Lett. **74**, 855 (1995).
- [3] J.D. Bjorken, Phys. Rev. D**47**, 101 (1993).
- [4] W. Buchmüller and A. Hebecker, Phys. Lett. B**355**, 573 (1995); W. Buchmüller, Phys. Lett. B**353**, 335 (1995).
- [5] O.J.P. Eboli, E.M. Gregores and F. Halzen, Phys. Rev. D**58**, 114005 (1998).

- [6] V. Del Duca and W.K. Tang, Phys. Lett. **B312**, 225 (1993).
- [7] R. Oeckl and D. Zeppenfeld, Phys. Rev. **D58**, 014003 (1998).
- [8] G. Oderda and G. Sterman, in preparation.
- [9] M. Derrick *et al.* (ZEUS Collaboration), Phys. Lett. **B369**, 55 (1996).
- [10] B. Harris and J.F. Owens, Phys. Rev. **D56**, 4007 (1997); H. Baer, J. Ohnemus and J.F. Owens, Phys. Rev. **D40**, 2844 (1989); J.F. Owens, Phys. Rev. **D21**, 54 (1980).
- [11] P. Aurenche, M. Fontannaz and J.P. Guillet, Nucl. Phys. **B286**, 553 (1987); Phys. Lett. **B338**, 98 (1994).
- [12] J.R. Forshaw and R.G. Roberts, Phys. Lett. **B319**, 539 (1993); L.E. Gordon and J.K. Storrow, Phys. Lett. **B291**, 320 (1992); D. Bödeker, Phys. Lett. **B292**, 164 (1992);
- [13] M. Drees and F. Halzen, Phys. Rev. Lett. **61**, 275 (1988); M. Drees and R. M. Godbole, Phys. Rev. **D39**, 169 (1989).
- [14] M. Klasen and G. Kramer Z. Phys. **C76**, 67 (1997); Z. Phys. **C72**, 107 (1996).
- [15] A. Levy, in *Lectures on QCD*, eds. F. Lenz, H. Griebhammer and D. Stoll (Springer-Verlag, Berlin Heidelberg, 1997), p. 347.
- [16] M. Derrick *et al.* (ZEUS Collaboration), Phys. Lett. **B384**, 401 (1996).
- [17] E. Gotsman, E. Levin and U. Maor, Phys. Lett. **B309**, 199 (1993), Phys. Lett. **B438**, 229 (1998), hep-ph/9902294.
- [18] C.F. Weiszäcker, Z. Phys. **88**, 612 (1934); E.J. Williams, Phys. Rev. **45**, 729 (1934).
- [19] S. Frixione, M.L. Mangano, P. Nason and G. Ridolfi, Phys. Lett. **B319**, 339 (1993).
- [20] J. Botts and G. Sterman, Nucl. Phys. **B325**, 62 (1989); M.G. Sotiropoulos and G. Sterman, Nucl. Phys. **B419**, 59 (1994); I.A. Korchemskaya and G.P. Korchemsky, Nucl. Phys. **B437**, 127 (1995).
- [21] N. Kidonakis and G. Sterman, Phys. Lett. **B387**, 867 (1996); Nucl. Phys. **B505**, 321 (1997); N. Kidonakis, G. Oderda and G. Sterman, Nucl. Phys. **B525**, 299 (1998); R. Bonciani, S. Catani, M.L. Mangano and P. Nason, Nucl. Phys. **B529**, 424 (1998).
- [22] N. Kidonakis, G. Oderda and G. Sterman, Nucl. Phys. **B531**, 365 (1998).
- [23] N. Kidonakis, E. Laenen, G. Oderda and G. Sterman, in preparation.

- [24] R.K. Ellis, W.J. Stirling and B.R. Webber, *QCD and Collider Physics* (Cambridge Univ. Press, Cambridge, 1996).
- [25] E. Laenen, G. Oderda and G. Sterman, Phys. Lett. B**438**, 173 (1998).
- [26] H.L. Lai *et al.*, Phys. Rev. D**55**, 1280 (1997).
- [27] M. Glück, E. Reya and A. Vogt, Phys. Rev. D**46**, 1973 (1992).
- [28] A.D. Martin, M.G. Ryskin and V.A. Khoze, Phys. Rev. D**56**, 5867 (1997).